D5.2 - Sensing electronics and control system for the submerged polymeric PTO

DATE: 10 May 2017

PROJECT COORDINATOR:
WavEC Offshore Renewables

GRANT AGREEMENT NR: 641334

The WETFEET – Wave Energy Transition to Future by Evolution of Engineering and Technology project has received funding from the European Union's Horizon 2020 programme under grant agreement No 641334.

Sensing electronics and control system for the submerged polymeric PTO			
Project	WETFEET – Wave Energy Transition to Future by Evolution of Engineering and Technology		
WP No.	5	WP Title	Submerged Polymeric PTO Breakthrough
Deliverable No.		5.2	
Nature (R: *Report*, P: *Prototype*, O: *Other*)		R	
Dissemination level (PU, PP, RE, CO)		PU	
Lead beneficiary:		SSSA	
Contributing partners		SSSA	
Authors List:		Marco Fontana, Giacomo Moretti, Francesco Damiani, Michele Righi	
Quality reviewer		Ana Novak, José Cândido	
Status (F: final; D: draft; RD: revised draft):		F	
Due Delivery Date:		30/04/2017	
Actual Delivery Date:		10/05/2017	

Version no.	Dates and comments
1	24 Feb 2017, definition of the preliminary structure of the report
2	12 Apr 2017, integration of contributes
3	26 Apr 2017, final version
4	10 May 2017, revised version
5	

Table of Contents

Table of figures

Table of tables

EXECUTIVE SUMMARY

This report is the Deliverable 5.2 of the WETFEET H2020 project. The document reports on the main activities conducted in the framework of the task 5.2

The main aims of this WP are: (1) the study and development of a power electronics and the associated sensing/control system for a PTO for WEC that is based on Dielectric Elastomer Generators (DEGs); (2) the study of effective controllers for DEG-PTO and (3) the design and development of a laboratory test-bench, employing the developed electronics and control algorithms, that is conceived to perform Hardware In the Loop (HIL) simulations.

DEGs are elastomeric electrostatic transducers that are able to directly convert the mechanical energy that is required to induce a deformation of their shape into medium voltage (5-10kV) DC electric energy. Preliminary study of this kind of devices in the context of wave energy sector have been conducted in the framework of the FP7 project PolyWEC. In such a project, the feasibility of the implementation of WECs based on DEG-PTO has been demonstrated through a set of small scale prototypes that have been tested in laboratory and wave-tank facilities. Such early works are characterized by the following limitations: (1) the electronics that has been employed was suitable for demonstration purpose but presented several limitations in terms of controllability of the devices and efficiency; (2) the submergence condition has been proved in the framework of laboratory tests at extremely small scale (1:75 i.e. dozen of milliwatts); (3) larger scale tests (with peak power of 3 W) have been conducted only in non-submerged conditions in wave-tanks with limitation in time and access; (4) sensing strategies were limited to indirect measures of air pressure to estimate the state and command the control.

The activities that are reported in this document are developed in this framework to advance the current status of development of such basic components of DEG-PTOs.

Specifically, the work was focused on the following main aspects:

- Study of power control electronics able to efficiently drive the DEG-PTO;
- Study of alternative sensing strategies that are needed for the control of the DEG-PTO in operational conditions;
- Implementation of a small-scale prototype (in the range of 3-10 W) of the sensing equipment and power electronics to be integrated in a HIL setup for the laboratory test of a fully functional DEG, i.e. a DEG that is actually able to efficiently convert mechanical oscillating energy into electricity;
- Study, in simulation environments, of the control strategies that have to be adopted in order to maximize the performance of the developed power and sensing systems.

In the first part of the document, the general problem of the control of a DEG-PTO is presented, in order to define the basic functionalities and specifications for the sensing and control electronics. In practice, this system should feature the following main functionalities:

- Power electronics should be able to efficiently perform the priming and energy extraction;
- The status of deformation of the DEG should be estimated in order to trigger the controller states;

In the following sections, the power electronics and sensing are studied. Several topologies have been considered and their choice was oriented towards a Dual Active Bridge Multilevel DC-DC converter that makes it possible to (1) fully cover the required functionalities, (2) achieve the required high efficiency in electrical energy transfer, (3) limit the number of (expensive) components including solid-states

switches and transformers/chokes, (4) use components that are rated with reduced maximum voltage that are largely available and cheaper.

The control strategies that make use of the designed power electronics and sensing are studied in simulation, demonstrating that an appropriate sub-optimal but effective control of the system can largely improve the performance of the device.

Beside these studies on sensing and power electronics, the control architecture of the HIL setup is also identified and integrated. Such architecture is based on a Matlab target machine that is able to handle the real-time simulation multi-DOF models of the linear hydrodynamics of WEC. Additionally, a first small scale (but up-scalable) prototype of DEG is developed according to a novel fabrication procedure. Such a prototype is assembled and tested on a preliminary laboratory setup.

LIST OF ACCRONYMS

DE	Dielectric Elastomers
DEG	Dielectric Elastomer Generator (to refer to the whole generator)
ECU	Elastomeric Conversion Unit (to refer to the sole DE membrane and conductive electrodes)
DAB	Dual Active Bridge
HIL	Hardware In the Loop
ICD-DEG	Inflated Circular Diaphragm Dielectric Elastomer Generator
LCOE	Levelized Cost of Electricity
MPC	Model Predictive Control
multi DOF	Multiple Degrees of Freedom
NS	Negative Spring
OPEX	Operational Expenditures
OWC	Oscillating Water Column
QP	Quadratic Programming
PD	Pressure Differential
PTO	Power Take-Off
SPC	Sensing, Power and Control
TRL	Technology Readiness Level
TPL	Technology Performance Level
WEC	Wave Energy Converter

1. Introduction

1.1. Dielectric elastomer control

In this section, we provide an introduction to the problem of control of WECs based on Dielectric Elastomer Generators (DEGs), providing a context of the work that is developed within the WETFEET project with respect to the state of the art.

The search and development of adequate control algorithms for WECs based on DEGs have to be conducted using dynamic modelling tool since generally there is a strong interaction between the DEG-PTO and the WEC hydrodynamics. Specifically, in WECs based on more conventional PTO, the presence of the PTO does not affect the overall stiffness of system; thus, the controller can be synthetized just to make it provide an appropriate damping to the primary mover. This approach cannot be pursued with DEG-PTOs that, due to their nature, provide a significant contribution to the stiffness in the dynamic response of the WEC, with the value of such a stiffness depending on the level of electrical activation.

For example, let us consider a series of incoming waves toward a generic DEG-based WEC device. In this system, the deformation of the DEG is influenced by the water motion but the amplitude of water motion is in turn affected by the deformation of the DEG. This means that when the DEG extracts energy, both the dynamics influence each other (that is, they are fully coupled). In this case, since electrical activation modifies the stiffness characteristic of the DEG (thus the overall system natural frequency), control operation could have also a contribute on the overall dynamics of the system. Thus, in order to synthetize and develop appropriate controllers, it is necessary to build an integrate a model of the system that takes into account the hydrodynamics, the elastic and electrical response of the DEG. This model has to include also the dynamic response of the power control electronics.

In previous work of some of partners involved in WP5, the generic control problem of a DEG-WEC has been theoretically considered for the architecture of the Oscillating Water Column WEC equipped with the Inflated Circular Diaphragm Dielectric Elastomer Generator (ICD-DEG). Such analysis considers an optimization approach that is based on validated models, however the conceived algorithms have not been tested on a real prototype. Actually, previous experimental works consider only demonstration prototypes that were developed for the validation of concepts but did not include all the essential features that are necessary to provide an effective test on the system controllers.

Differently, in the activities of WP5 of WETFEET project, one of the final aim is the development of a setup that enables the experimental testing of a scaled DEG-PTO in fully functional operation i.e. equipped with the following new features:

- fully functional sensing and power electronics;
- real-time hardware in the loop controllers and hydrodynamic models that are suitable to represent also the submerged case;
- possibility of evaluating the global efficiency of the system;
- high quality DEG-PTO prototype fabricated according to a repeatable and reliable procedure;

In the following section a brief description of the generation cycle of a generic DEG is presented in order to explain the basic working principle and define the generic functionalities that are required to the sensing and control electronics to be able to perform such cycles.

1.1.1. DEG generation cycle

With regard to the control law, and based on the aforementioned operational constraints, we now recall the principal ways to extract energy from DEGs.

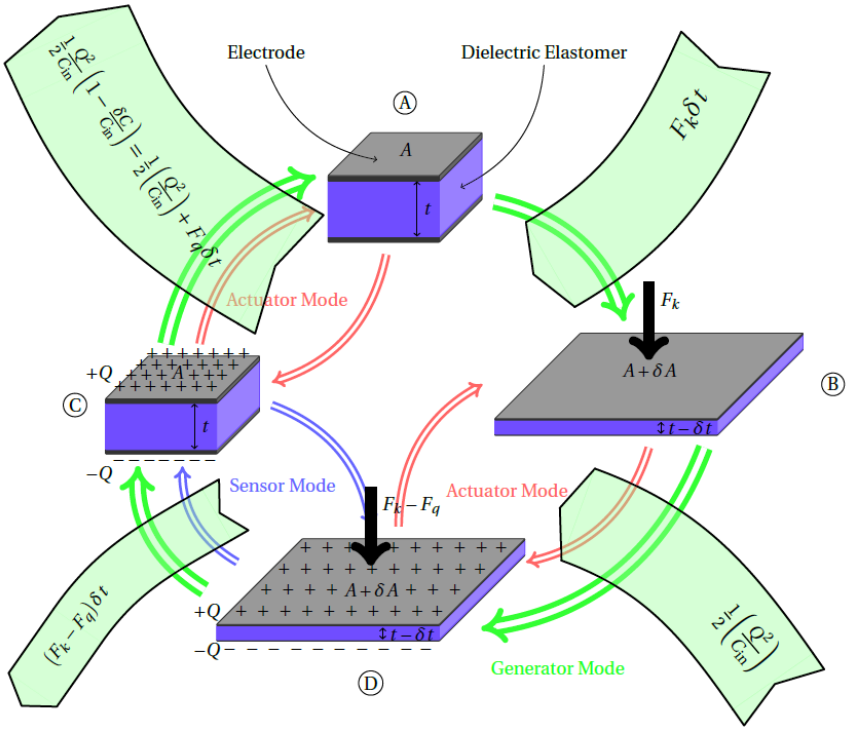

FIGURE 1-1 DIELECTRIC ELASTOMER WORKING PRINCIPLE. THE RED ARROWS INDICATE HOW THE DE WORKS AS ACTUATOR; THE BLUE ARROWS SHOW HOW IT WORKS AS A SENSOR AND THE GREEN ARROWS DENOTE HOW IT WORKS AS GENERATOR, CONSIDERING A CYCLE WITH A CONSTANT CHARGE.

The basic phases and concepts of DEG working principle are reported in Figure 1-1, where Q represents the amount of charge on the electrodes, C represents the capacitance of the DEG (C_{in} being the capacitance of the membrane in the deformed state), F_k is the compressive force applied on the DEG surface and F_q is the electric force due to the charge.

Considering the electrostatic potential energy stored in the DE electric field, U_{le}, and the electric work performed on the DEG by the external circuit, W_{el}, the infinitesimal energy extracted by the DEG in correspondence to an infinitesimal deformation is

$$dW_{DEG} = dU_{le} - dW_{el} \tag{1.1}$$

where dU_{le} and dW_{el} can be obtained from an energy balance equation that reads as follows:

$$dW_{DEG} = \frac{V^2}{2}dC + VCdV - V^2dC + VCdV = -\frac{1}{2}V^2dC, \tag{1.2}$$

where dV and dC represent the generic infinitesimal variations of voltage V and capacitance C, respectively. From equation (1.2), it can be seen that electricity is positively generated when $dC < 0$.

That is, the DEG behaves as a generator (producing a positive electrical energy output) if it is electrically activated while its capacitance decreases. Therefore, to harvest energy out of the deformation of the DEG, the voltage across the DE electrodes needs to be properly regulated.

Referring to the *Q*-*V* plane, a generic control pattern followed by the generator in a cycle is represented by any closed curve included within the physically allowable operating space. The area enclosed by the considered curve is numerically proportional to the mechanical energy converted into electrical energy in that cycle, which is given by

$$W_{DEG} = \oint \mathrm{d}W_{DEG} = -\oint V \mathrm{d}Q \tag{1.3}$$

In particular, the limiting curves define a cycle, which encloses an area equal to the maximum energy that can be converted in a single cycle by the DEG (see Figure 1-2). With reference to this figure, the generation cycle is controlled as follows. In State 1 the DEG is kept inactive during its expansion, i.e. the capacitance increases. This part of the cycle is not visible in the Q-V plane because it collapses in the axes origin. In state 2, the control is activated when the membrane reaches the maximum deformation. This phase is identified by red arrows (from O→E). The control law is followed in order to obtain the chosen strategy. This phase is identified by blue arrows from E→F. The DEG is discharged when the capacitance is minimum, that is, when the ICD-DEG is flat. This phase is identified by black arrows from F→O. The different control strategy features the following attributes:

- **Constant Charge** (see Figure 1-2-a). This control scheme is based on putting a fixed amount of charge on the electrodes when the capacitance is maximum and then extracting the same amount of charge at a higher voltage. This control strategy is very simple to implement, but the amount of energy that can be extracted with respect to the feasible physical region is poor. Some experimental results using this kind of control scheme were reported in [19]
- **Constant Voltage** (see Figure 1-2-b). In order to obtain this control strategy, it is necessary to connect a battery to the electrodes when the capacitance decreases. This control scheme is easy to implement, but requires choosing the right voltage depending on the stretch in order to reach high energy extraction levels.
- **Electric Field Control** (see Figure 1-2-c). This control strategy tries to maximise the energy harvested in the cycle. The scheme consists in choosing the right voltage to be imposed between the electrodes as:

$$\bar{V}(\lambda) = \bar{E}t(\lambda) = \beta E_{BD} t(\lambda) \tag{1.4}$$

where t is the thickness of the membrane, $\bar{E}$ is the electric field applied across the DEG and β is a safety factor. This strategy requires the knowledge of the thickness value in order to obtain the right voltage to be impose between the electrodes. This information can be obtained by using other information, such as the DEG tip elevation or its capacitance value.

- **Feasible physical region.** This control scheme maximises the energy harvested in the cycle. It is based on the following law

$$V(\lambda) = \beta \min(V_{\sigma_0}(\lambda), V_{E_{BD}}(\lambda)) \tag{5}$$

where $V_{\sigma_0}(\lambda)$ is a function that returns the exact value of voltage that verifies the bucking and $V_{E_{BD}}(\lambda)$ is a function that returns the exact value of voltage that verifies the breakdown condition of the membrane. Both functions require the knowledge of the actual value of stretch, λ, of the DEG. For this reason, execution of this control scheme is very difficult if the characteristics of the material are unknown.

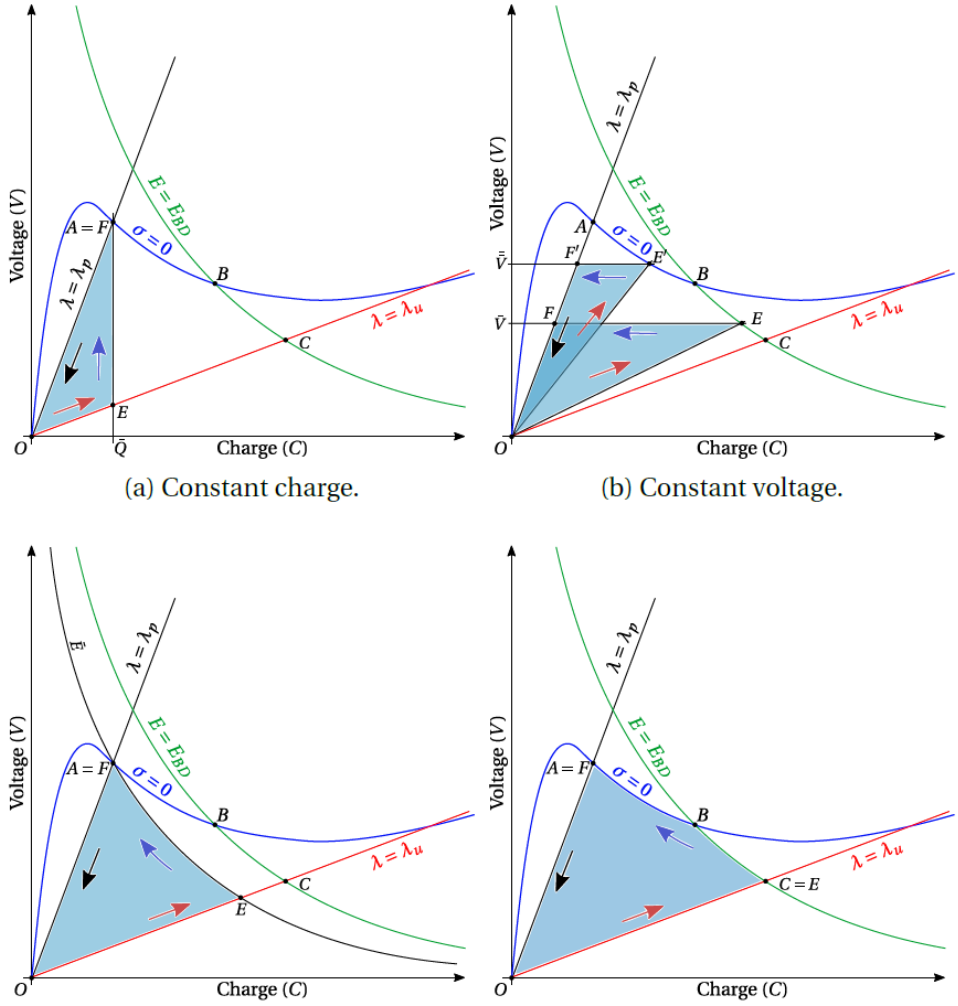

FIGURE 1-2 Q-V PLOTS OF THE BASIC GENERATION CYCLES:

All the control strategies presented here are based on a specific path in the *Q-V* plane. However, all of them use the concept of a basic four phase control scheme with the following main steps:

1. The DEG is kept inactive during its expansion, when the capacitance increases. This part of the cycle is not visible in the *Q-V* plane because it collapses in the plane's origin. This phase is called "inactive phase".
2. When the membrane reaches its maximum deformation, the control is activated. In Figure 1-2, this phase is identified by the red arrows (from O→E). This phase is called the "charging phase".
3. The control law is followed in order to obtain the chosen strategy. This phase is identified by the blue arrows from E→F. This phase is called "harvesting phase" or "active phase".
4. The DEG is discharged when the capacitance is minimal (namely, when the DEG is flat). This phase is identified by the black arrows from F→O. This phase is called "discharging phase".

More generally, voltage and charge of the DEG can be controlled according to closed loops in the *Q-V* plane, having each cycle corresponding to an amount of energy converted that is proportional to the enclosed area.

1.2. Definition of Functionalities of Sensing, Power and Control Electronics

On the basis of the previous description of the ideal generation cycles of a DEG, we can define the basic functionalities that are required to the sensing, power and control (SPC) system to be able to automatically operate.

Specifically, these are the basic functionalities that should be implemented during the cyclical operation:

(1) *Measure and elaborate* the status of deformation (or capacitance, since they are linked) of the DEG in order to decide instantaneously about the charging status of the device. This can be achieved in different ways. An indirect method was proposed and tested in previous studies on DEGs that are based on the ICD-DEG architecture. For these devices the electrical activation of the DEG can be easily decided on the basis of the measure of the pressure and the calculation of its derivative. In the case of submerged DEG, the issue can be solved through the technique of the self-sensing that is implemented and described in the following sections of this document.

(2) *Bidirectional charging-discharging:* the flux of charge on the DEG needs to be bidirectional since the loops in the *Q-V* plane must be closed. This functionality has not been implemented previously with effective solutions. In previous studies, the employed electronics was developed for the purpose of demonstration and its unfavorable contribution to the global performances of the DEG-WEC was ignored (i.e., performance analysis was restricted to the consideration of the amount of electrical energy generated by the DEG, regardless of the successive dissipation in the conditioning circuit). In this document, we describe the study and the implementation of a high efficiency electronics that is potentially able to implement energy cycles with efficiency in the order of 90-95%.

1.3. Contents of the document

This document is organized as follows. Section 2 provides a description of the design process of the power electronics and the sensing strategies. Section 3 studies control strategies that are intended to exploit the designed power electronics (considering its limiting aspects). Section 4 provides a summary

of the work done toward the design of the HIL setup that makes it possible to implement the designed systems in a laboratory scale.

2. Power and sensing electronics

2.1. Introduction

As briefly analysed in Section 1, the basic functionalities of the SPC system are to *measure* (sense) the status of deformation and to consequently *control* the status of activation of the DEG during its cyclical operation.

Several circuit topologies for power control of DEG have been proposed in the literature. However, most of these circuital concepts have the sole purpose to demonstrate the energy produced within one or more generation cycles disregarding the real/global power efficiency of the conversion system [24] or they assume architectures that can be effectively implemented at very small scales but cannot be scaled up (to hundred of kilowatts level).

All those circuits are not suitable for the control of a DEG in a real context of wave energy conversion. A study on a possible architecture that can be employed for the power controller of a DEG that can feature high efficiency suitable for realistic application is the Bidirectional Modular Multilevel DC-DC Converter [1]. In this work, the authors have studied a topology based on a stacked of Bidirectional DC-DC converters connected in series on the DEG side and in parallel on the load side (e.g., the electric grid side), as shown in Figure 2-1. This allows the application of high voltage on the DEG (10kV) and while keeping a lower voltage on the load (800V).

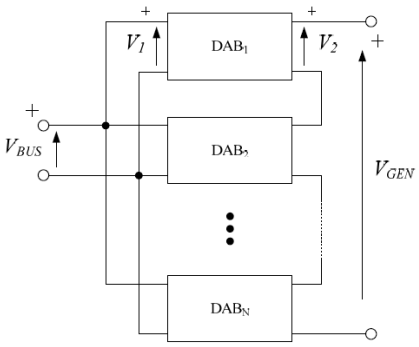

FIGURE 2-1: MULTILEVEL DC-DC CONVERTER TOPOLOGY

Every single module is a Dual Active Bridge (DAB) (Figure 2-2) which is a circuit largely used in power management applications because of its high efficiency (>90%) and because it allows to transfer power on both directions. This kind of circuit is used also in electric or hybrid vehicles, fuel cells and in other renewable energy applications.

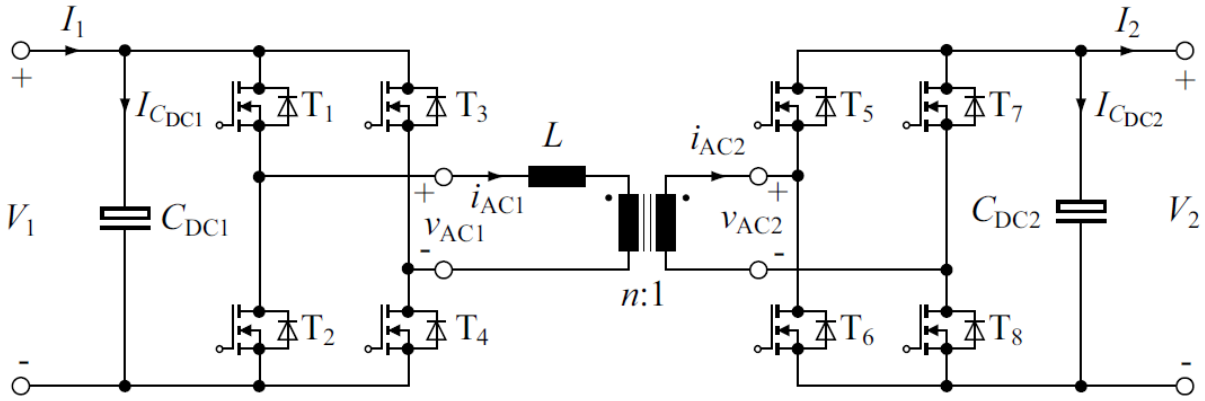

FIGURE 2-2 : DAB CIRCUIT SCHEMATIC

In addition, the DEG needs a sensing strategy to be controlled. Specifically, in order to decide the instant in which the DEG-PTO should be activated (priming), the deformation status of the DEG membrane has to be estimated. This can be achieved indirectly, measuring the tip position or, in the OWC application, the pressure inside the air chamber (as reported in [19]). Tip position and pressure versus capacitance characterization gives an easy way to control charging and discharging of the DEG. However a more general approach is to directly measure the capacitance in real time. This sensing strategy is much more versatile and can be applied also to different types of WEC (for example, submerged systems) and DEG topologies, as further discussed below.

2.2. Power electronics

In the following subsection, the different topologies of power circuits that can be employed for the control of DEG-PTO are analysed. Thereafter design considerations are drawn in order to define procedures for the dimensioning of the circuit.

2.2.1. Topologies

Many different electronic circuit topologies can be proposed to manage energy generation from a DEG. First of all, the focus must be set on the type of electrical output source that we want to provide (either AC or DC). The DEG works with DC voltages, this brings immediately to the choice of DC power as output of our electronic circuit. DC voltage is suitable for driving loads and for DC grids. DC grids are widely used in renewable energy such as wind farms. This kind of electric power can be converted anyway into AC power using inverters. In this work, we restrict to consider DC power production, regardless of eventual successive transformations. For this reason, DC power converters will be investigated.

DEG energy generation is discontinuous, this means that to adapt this kind of generator to a load or to the grid, a DC-link capacitor or battery must be used. The DC-link allows to provide continuous power to the load using discontinuous power provided from the DEG. In addition, the DEG is charged and discharged within a generation cycle. Choosing a DC-link capacitor big enough, the charging and discharging of the DEG can be obtained limiting the ripple on the load side. As a result, our circuit must be able to transfer charge to and from the DEG allowing to perform the generation cycle. The most efficient way to perform this energy transfer is to use switching DC-DC converters. Series DC power regulators (see Figure 2-3) are to be excluded, because series elements dissipate energy giving poor performance in terms of efficiency.

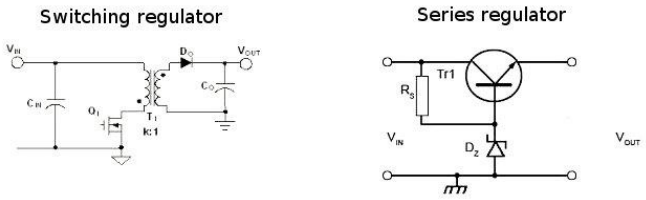

FIGURE 2-3 CONVERTERS, SWITCHING VS SERIES REGULATORS.

Switching DC-DC converters can be divided into two large families: non-insulated and insulated switching DC-DC converters. In the first category, the main topologies are buck, boost, buck-boost converters.

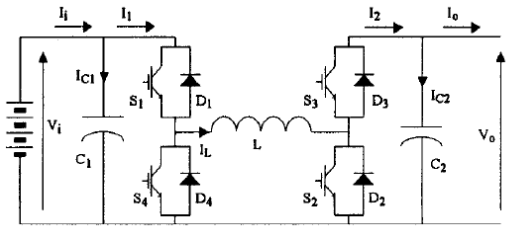

FIGURE 2-4: BIDIRECTIONAL BUCK-BOOST SWITCHING CONVERTER

Figure 2-4 shows the bidirectional buck-boost converter, which is the only not insulated converter that allows to transfer power on both directions. However, this topology is not suitable for modular multilevel DC-DC converters because the modules on the DEG side are required to be connected in series, i.e. on the secondary side of the converter the voltage must be floating with respect to the primary side, where the modules are connected in parallel. For this reason, is necessary to adopt an insulated switching DC-DC converter topology.

There are several topologies of insulated switching converters which are bidirectional such as flyback, forward-flyback, half bridge, full-bridge. The last one offers better performance in terms of efficiency. Despite the complexity and increased cost of this solution, it offers better performance over a wide range of working conditions and makes the full bridge bidirectional converter the best choice for DEG application.

The DAB key component is the transformer, which guarantees insulation between the DEG and the load and allows to transfer power from and to the membrane. The power transfer is performed switching the DC voltage through Mosfets mounted in full bridge configuration. Controlling the two full bridges duty cycles and phase difference, it is possible to transfer power on both directions. The choice of DAB working voltage is limited by the Mosfets maximum ratings. Although some high voltage (4500V) Mosfets can be found, these are not suitable for our application because the Mosfet high-side drivers are not available for such voltages. This allows to realize only topologies with low-side Mosfets such as flyback or forward switching converters. Despites their simplicity and lower cost, these topologies have lower efficiency. Another crucial aspect to be considered regards the transformer. Increasing the converter working voltage, the number of turns of the transformer increases. The series inductance of the transformer increases with the squared number of turns. The increase of inductance is a limitation to the maximum power transferrable from the primary to the secondary. The choice of 800V working voltage will be discussed further. The DAB modules will be connected in series to obtain a DEG working voltage >6kV, this means that the Multilevel DC-DC converter will be made of 8 modules. In case a higher voltage is required, it is necessary to just add more modules.

2.2.2. Multilevel DC-DC

Before studying the multilevel DC-DC converter in depth, a detailed analysis of the DAB must be presented. The Multilevel DC-DC converter that is studied here is based on several specifications such as DEG dimension, efficiency requirement, expected power generation, and DEG operative voltage. Assuming a target power of 4W, we suppose to use a membrane with 400mm diameter made of two layers of acrylic material (VHB 4905, by 3M), each with a thickness of 1mm (in the unstretched configuration), pre-stretched by 3.5 times. This brings to a capacitance range of the DEG which varies between 100nF and 500nF. From the geometry of the DEG, it comes that the peak voltage of the membrane will be roughly 6kV. The duration of the charging and discharging phases is another constraint to be considered. The membrane descripted above represents a scaled PTO of the WEC at a scale of approximately 1:30. The period of the waves at such a scale is about 1Hz (considering Froude-scaled sea waves). We suppose to charge and discharge the membrane within 1/100 of the period, which means 10ms. The charging of the membrane occurs when the DEG reaches maximum capacitance. To charge a capacitor to 6kV within 10ms a current of 40mA is needed. This gives the maximum power requirement of 32W. This is the worst working condition of the converter. To obtain an efficiency >90% the maximum power loss is supposed to be 3W. Since the Mosfet's R_{dsON} is very low (>30mOhm) the power loss is concentrated in the transformer. It can be demonstrated that the maximum efficiency of a transformer is achieved when the core loss is equal to the copper loss [3]. The required core loss is >1.5W. The switching frequency is another point to be considered. The datasheet of a reference ferrite (3C90 Ferroxcube) shows the power loss versus flux density at different switching frequency. The higher the frequency the lower the flux density at the same power loss. That's why the chosen frequency is f=100kHz. To achieve the desired power loss, the needed flux density 180 mT. A lower flux density gives less hysteresis. The DAB voltage at the load side is equal to the voltage on the DEG side and is 800V which means that the turns ratio of the transformer is 1:1. The number of turns is easily calculated using the Faraday-Newman-Lenz law.

$$N = \frac{V\, t_{on}}{B_{max}\, A} \tag{2.1}$$

where A is the core cross section, and t_{on}=1/f. From the number of turns and the filling factor, it is possible to calculate the gauge of the copper wire, the copper resistance and the inductance of each winding. This is useful to calculate the maximum current variation on the primary circuit at the selected switching frequency.

$$I_{max} = \frac{V\, t_{on}}{L_{prim}} \tag{2.2}$$

If the inductance is not too high the current swing into the primary of the transformer allows to transfer the required power to the secondary. This can be seen from the formula:

$$P_{max} = \frac{{I_{max}}^2\, L_{prim}\, f}{2} \tag{2.3}$$

In conclusion, the power transferred from the transformer will be 35W which is enough to charge the membrane in the required time. As told before, the choice of 800V as switching frequency comes from several factors. Firstly, the transformer should have many more turns at higher voltages, which means higher inductance. In addition, the insulator on the windings' wire must be thicker, thus subtracting room to the copper within the transformer assembly. This gives a higher copper loss. Secondly the available switching Mosfets have a considerably lower R_{dsON} at 800V instead of higher voltage devices. As an example, 4.5kV-Mosfets are available, which have R_{dsON}=60Ω instead of 22 mΩ of the 1.2kV-

Mosfets chosen for our application. The latter also offers better performance in terms of leakage current and gate charging characteristics.

The Mosfet switching commands are provided from drivers insulated from the microcontroller side through photocouplers. The insulation must be guaranteed because in a multilevel topology every DAB works at different voltage.

Many different control strategies can be applied to the DAB. Basically, the choice of Mosfet switching time on both sides of the DAB will give different effects. As shown in Figure 2-5, there are four parameters which can determine the power transfer in DAB:

- Switching frequency f_s
- Duty cycle of primary D_1
- Duty cycle of secondary D_2
- Phase shift between primary and secondary φ

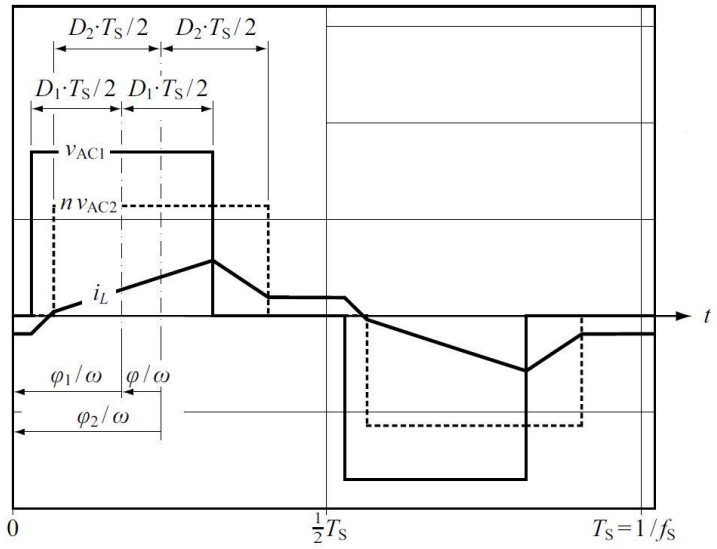

FIGURE 2-5: EXAMPLE OF CONTROL PARAMETERS SEQUENCE

The control strategies discussed in this chapter are focused on two main tasks. The charge and discharge of the DEG at the beginning and at the end of the generation cycle, and the power transfer throughout the entire generation cycle. The first task is performed exploiting the maximum power transferable by the DC converter. The best choice in this case should be a constant power charging strategy. Charging a capacitor with constant power source is one of the most efficient methods. The capacitance to be charged is:

$$C = \frac{Q}{V} \tag{2.4}$$

The power is given by:

$$P = VI \tag{2.5}$$

Combining the two equations yields to:

$$P = V(t)C\frac{dV(t)}{dt} \tag{2.6}$$

Thus:

$$V(t) = \sqrt{\frac{2Pt}{C}} \tag{2.7}$$

Integrating the power provided over time, the energy spent from instant zero to instant t is:

$$Pt = \frac{1}{2}CV(t)^2 \tag{2.8}$$

The energy spent to charge the capacitor is exactly equal to the energy stored. This means that no dissipation occurs during the charging process. Anyway, under a certain voltage the constant power charge is not feasible because the current would be infinite. In practice the charging of the capacitor will be performed at constant current first . When voltage is high enough, the charging will occur at constant power.

In order to understand the basic working principle of the DAB, a simplified model can be analysed. Thus the voltage across the primary and secondary can be replaced with voltage sources and the transformer can be replaced [2] with the series inductance as shown in Figure 2-6.

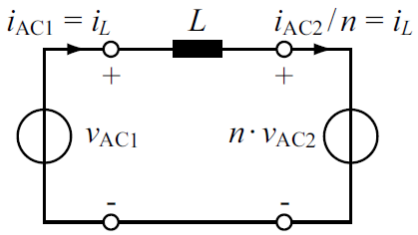

FIGURE 2-6: DAB SIMPLIFIED LOSSLESS EQUIVALENT CIRCUIT

In our case the number of turns can be set to 1 just to simplify our considerations. Voltage across primary can have three possible levels:

$$v_{ac1}(t) = \begin{cases} +V_1, \ T_1, T_4 \ ON, T_2, T_3 \ OFF \\ 0, \ T_1, T_3 \ ON, T_2, T_4 \ OFF \\ 0, \ T_2, T_4 \ ON, T_1, T_3 \ OFF \\ 0, \ T_1, T_2, T_3, T_4 \ OFF \\ -V_1, \ T_1, T_4 \ ON, T_2, T_3 \ OFF \end{cases} \tag{2.9}$$

Similarly, $v_{ac2}(t)$ can be equal to $+V_2, 0, -V_2$ depending on T_5, T_6, T_7, T_8. The resulting voltage $v_r(t)$ is the difference between $v_{ac1}(t)$ and $v_{ac2}(t)$. Thus the current flowing through the inductor is:

$$i(t) = i_L(t_0) + \frac{1}{L}\int_{t_0}^{t} v_r(t)\, dt \tag{2.10}$$

This allows to express the instantaneous power on primary and secondary:

$$p_1(t) = v_{ac1}(t)\, i_L(t) \tag{2.11}$$

$$p_2(t) = v_{ac2}(t)\, i_L(t) \tag{2.12}$$

Averaging over a period T_s:

$$P_1 = \frac{1}{T_s}\int_{t_0}^{t_0+T_s} p_1(t)dt \tag{2.13}$$

$$P_2 = \frac{1}{T_s}\int_{t_0}^{t_0+T_s} p_2(t)dt \tag{2.14}$$

Our model is assumed to be lossless. The consequence of this is:

$$P_1 = P_2 \tag{2.15}$$

This balance is the basis of the control strategies we are going to explain.

The simplest between DAB control principles is the Phase Shift Modulation. The frequency is kept constant and the duty cycles of the two full bridges is maximum (D1=D2=50%). The only control variable is the phase shift φ. As shown in Figure 2-7 the power can be easily calculated:

$$P_1 = \frac{1}{T_s}\int_0^{T_s} p_1(t)dt = \frac{2V_1}{T_s}\int_0^{\frac{T_s}{2}} i_L(t)dt \tag{2.16}$$

In order to calculate i_L the semi-period is divided into two intervals:

Interval 1: $$i_L(t) = i_{L,0} + (V_1 + V_2)\frac{t}{L}; \quad 0 < t < T_\varphi \tag{2.17}$$

Interval 2: $$i_L(t) = i_{L,T_\varphi} + (V_1 + V_2)\frac{t-T_\varphi}{L}; \quad T_\varphi < t < \frac{T_s}{2} \tag{2.18}$$

Due to the half cycle symmetry:

$$i_{L,0} = \frac{\pi(V_2-V_1)-2\varphi V_2}{4\pi f_s L} \tag{2.19}$$

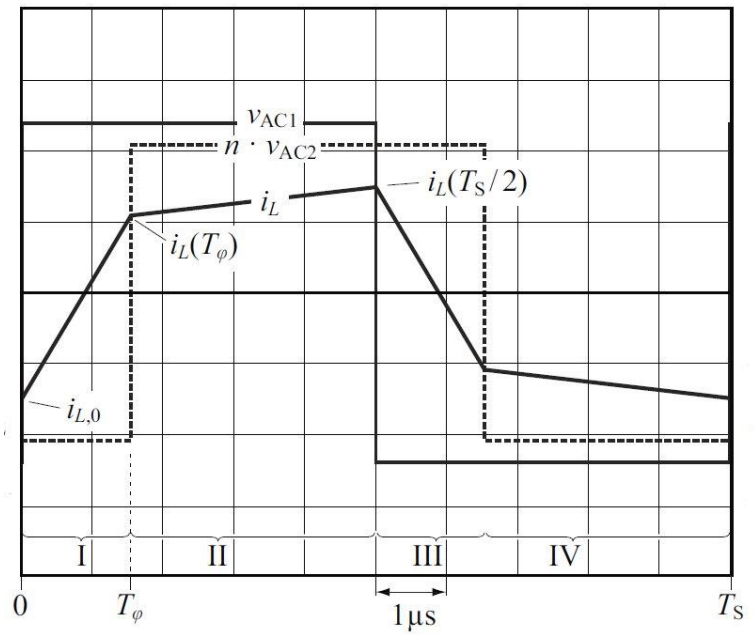

FIGURE 2-7 :PHASE SHIFT MODULATION SEQUENCE EXAMPLE

The transferred power becomes:

$$P = P_1 = P_2 = V_1 V_2 \varphi(\pi - |\varphi|); \qquad -\pi < \varphi < \pi; \tag{2.20}$$

When P is positive the power is transferred from primary to secondary and when P is negative the power is transferred in the other direction. The maximum power transfer is achieved when:

$$P_{MAX} = \frac{V_1 V_2}{8 f_S L} \tag{2.21}$$

The calculated maximum power in our case is 36W as expected. Whit this control strategy the φ is set to achieve a desired power output using the formula:

$$\varphi = \frac{\pi}{2}\left[1 - \sqrt{1 - \frac{8 f_S L|P|}{V_1 V_2}}\right] sgn(P) \tag{2.22}$$

Besides its simplicity this control strategy there are some disadvantages like a limited operating range and large amount of transformer RMS current. Switching losses are also high since ZVS and ZCS are not applied. This makes phase shift modulation suitable for fast charge and discharge but not for DEG generation cycle where is required to manage small currents.

Triangular Current Mode Modulation is another possible control strategy. The principal advantage respect to the previous one is due to the ZCS which minimize switching losses. The control variables in this case are D_1 ,D_2 and φ. Frequency is kept constant in this case. The maximum power is achieved with $T_3 = 0$ which gives the maximum current excursion:

$$P_{max} = \frac{n^2 V_2^2 (V_1 - n V_2)}{4 f_S L V_1} \tag{2.23}$$

Notice that in our case $n = 1$.

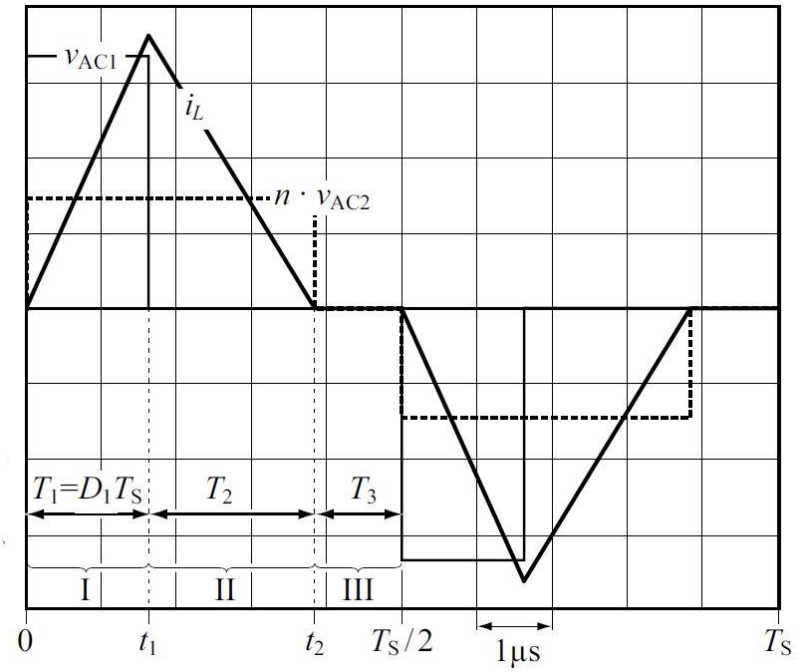

FIGURE 2-8 : TRIANGULAR CURRENT MODE MODULATION SEQUENCE EXAMPLE

To obtain power transfer in the opposite direction the current must be controlled as shown in Figure 2-9.

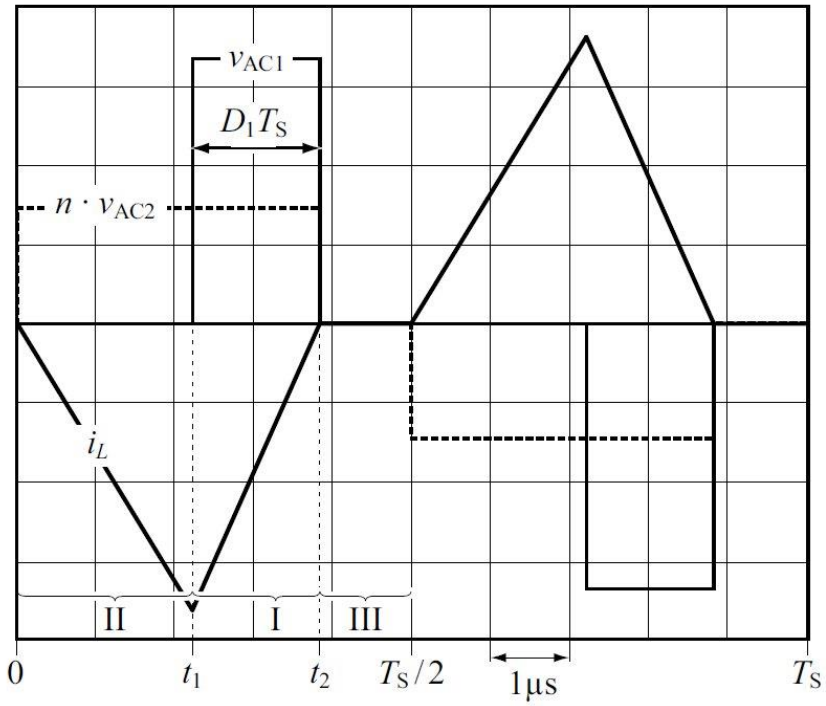

FIGURE 2-9: TRIANGULAR CURRENT MODE MODULATION SEQUENCE EXAMPLE

Reverse power transfer

Same consideration can be made about maximum power. It should be noticed that value of current at switching instant is zero. This gives advantage in terms of switching loss. Nevertheless, the transferable power is lower with respect to the phase shift control method in this case is easier to perform a fine control of power transfer. That makes this control strategy suitable for low current and low power applications. In this case, power transfer is not possible when $V_1 = V_2$.

$$P_{max} = \begin{cases} \frac{n^2 V_2^2 (V_1 - nV_2)}{4 f_s L V_1} \; ; \; V_1 > nV_2 \\ 0 \; ; \qquad V_1 = V_2 \\ \frac{V_1^2 (nV_2 - V_1)}{4 f_s L n V_2} \; ; \; V_1 < nV_2 \end{cases} \tag{2.24}$$

To avoid this undesirable behaviour when $V_1 \sim nV_2$ the Trapezoidal Current Mode Modulation can be taken into consideration. This control strategy can be performed either at ZCS or not. This makes this method more flexible and suitable for different working conditions.

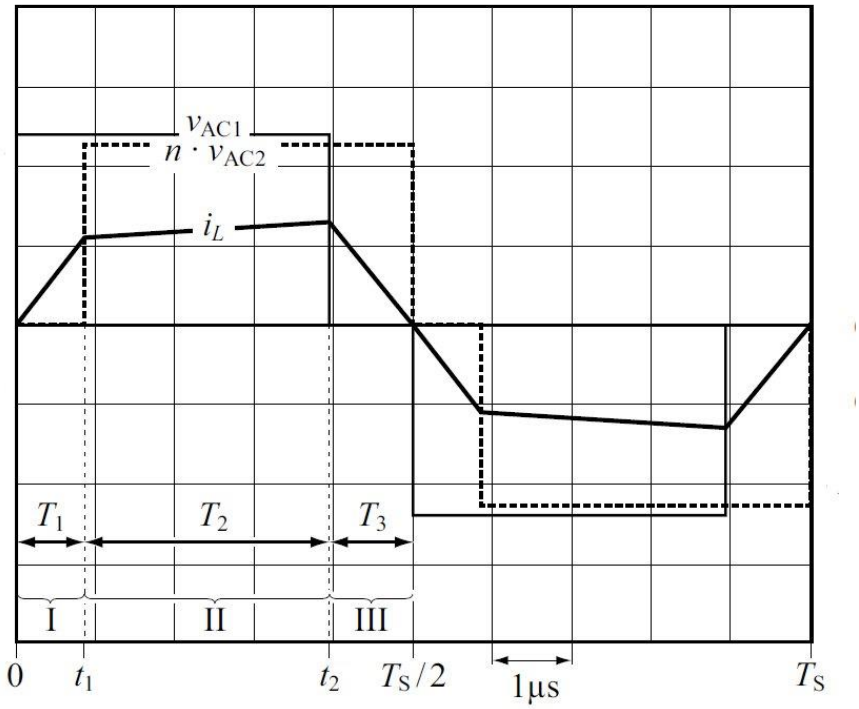

FIGURE 2-10: TRAPEZOIDAL CURRENT MODE MODULATION SEQUENCE EXAMPLE

Figure 2-10 shows the working principle of trapezoidal current mode modulation this method employs duty cycles and φ to perform the power transfer from one side to the other of the DAB. The value of maximum power transferable is:

$$P_{max} = \frac{(nV_1V_2)^2}{4f_sL(V_1^2+nV_1V_2+(nV_2)^2)} \tag{2.25}$$

This control strategy allows to transfer more power with less RMS inductor current it also can work with ZCS giving better performance in terms of efficiency respect to the methods shown before.

In order to achieve the minimum possible losses the Optimal Mode Modulation can be taken into consideration. The aim of the optimal modulation is to minimize the inductor current. This method is in a way a hybrid of all the previous shown before. To better understand the philosophy at the base of optimal modulation let's show a set od 12 possible control sequences for a certain voltage level and frequency.

The optimal analysis shows that the increase in inductor current is not necessarily related to an increase of power output. The optimization procedure then minimizes the cost function, e.g. the value of the RMS current IL, with respect to D1 and D2 for a fixed operating point in order to determine the optimal modulation scheme.
The result of the optimization process in terms of control variables are illustrated below, the optimum parameters that minimize inductor current can also be calculated analytically [2].

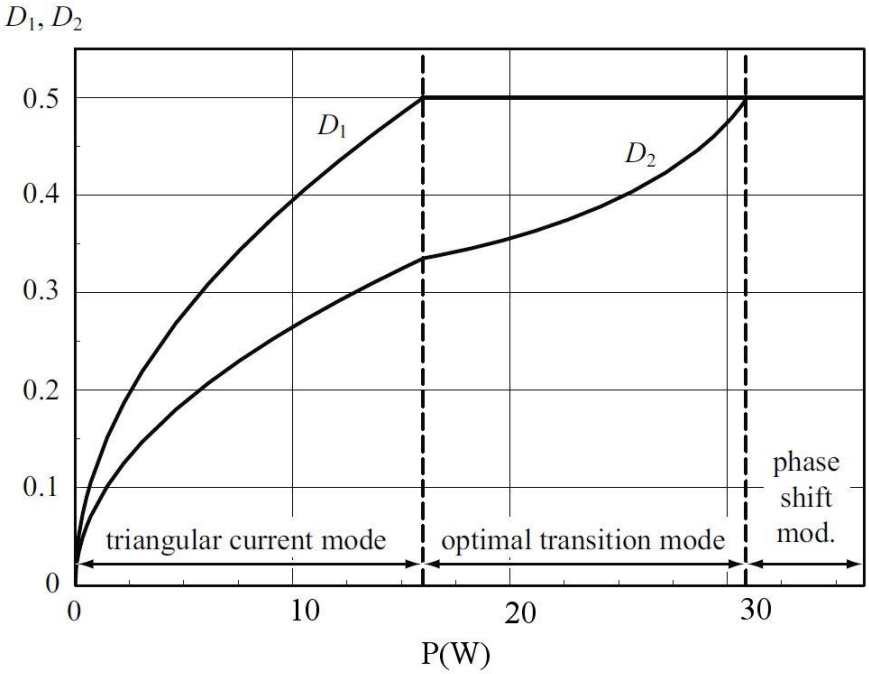

FIGURE 2-11: OPTIMAL DUTY CYCLES THAT MINIMIZE RMS CURRENT

As shown in Figure 2-11 the phase shift modulation is optimal for hi power output. On the other hand, the triangular current mode results to be optimal to transfer small amount of power. For medium power applications, the DAB works in the optimal mode and the duty cycle values can be calculated analytically.

The lossless model has been investigated so far. This is useful to understand which control strategy will be chosen in every working condition of the DAB. In our particular application, the circuit is going to work at high power rating and at very low power ratings. For this reason, the chosen control methods will be phase shift modulation when charging and discharging the DEG and triangular when generating.

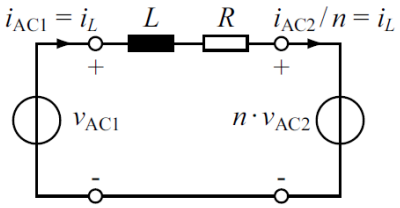

FIGURE 2-12: CONDUCTION LOSS CONVERTER MODEL

In order to explain the complete model including conduction losses and core losses a more complex discussion has to be done. Firstly, the equivalence $P_1 = P_2$ is no longer true because of losses. For example, the phase shift modulation expression of power becomes:

$$P_{in} = \left\{\frac{(V'_{in})^2}{R}\left[1 - 4\tau f_s \tanh\left(\frac{1}{4\tau f_s}\right)\right] - \frac{V'_{in}V'_{out}}{R}\left[1 - \frac{2\varphi}{\pi} + 4\tau f_s \sinh\left(\frac{|\varphi|}{2\pi\tau f_s}\right)\right] - \frac{4V'_{in}V'_{out}\tau f_s}{R}\left[2sinh^2\left(\frac{|\varphi|}{4\pi\tau f_s}\right)\right] + \frac{4V'_{in}V'_{out}\tau f_s}{R}\left[e^{\frac{|\varphi|}{2\pi\tau f_s}} tanh\left(\frac{1}{4\tau f_s}\right)\right]\right\} sgn(\varphi) \quad (2.26)$$

$$P_{out} = \left\{\frac{(V'_{out})^2}{R}\left[4\tau f_s tanh\left(\frac{1}{4\tau f_s}\right) - 1\right] + \frac{V'_{in}V'_{out}}{R}\left[1 - \frac{2|\varphi|}{\pi} + 4\tau f_s sinh\left(\frac{|\varphi|}{2\pi\tau f_s}\right)\right] - \frac{4V'_{in}V'_{out}\tau f_s}{R}\left[2sinh^2\left(\frac{|\varphi|}{4\pi\tau f_s}\right)\right] - \frac{4V'_{in}V'_{out}\tau f_s}{R}\left[e^{-\frac{|\varphi|}{2\pi\tau f_s}} tanh\left(\frac{1}{4\tau f_s}\right)\right]\right\} sgn(\varphi) \quad (2.27)$$

where $\tau = \frac{L}{R}$.

In this case, the maximum power transfer is no longer obtained with $\varphi = \frac{\pi}{2}$ but the useful range of control for this strategy is quite less. In addition, the closed-form expression of φ respect to a desired power output doesn't exist. This means that the controller must use a numerical solver to calculate the value of φ from the equation above. Once again for triangular and trapezoidal modulation schemes the closed-form expression of D1 D2 and φ doesn't exist. A numerical solver is needed also in this case.

The different working conditions need to be treated separately. The first is the charging of the DEG. As told before is desirable to charge at the maximum power. When the DAB receives, a charging trigger the control scheme is set on phase shift method which allows the maximum power transfer. The phase shift is set near $\frac{\pi}{2}$. The control structure of DAB in general is composed of two nested control loops, the inner adjusts the inductor current and the outer regulates the output voltage. During charge the outer loop is out of control. When the charge is completed, the output voltage set point is reached and the control passes from the inner loop to the outer. The controller changes to triangular current mode modulation and follow the output voltage set point. This is the generation phase. The controller regulates the current in the opposite direction to get power from the DEG. When the generation phase is completed, the discharge event is triggered. The strategy is the same as in charging with the only difference that φ is negative. The discharge will be as fast as possible exploiting the maximum power of the DAB in phase shift mode. Furthermore, an external control loop will control the DEG generation cycle providing the voltage set point to the underlying voltage control loop as shown in Figure 2-13.

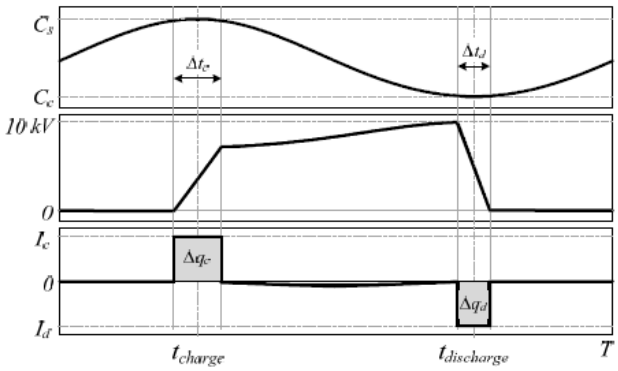

FIGURE 2-13: DEG GENERATION CYCLE

The multilevel DC-DC converter is made from a stack of DAB modules. The outer control loop must synchronize every single module. To do this there are mainly two strategies: parallel and bypass.

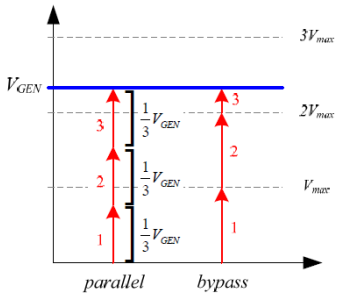

FIGURE 2-14 : MULTILEVEL DC-DC CONVERTER CONTROL STATEGIES

As shown in the example Figure 2-14 in parallel mode the output of every DAB is modulated in order to achieve the desired voltage. The bypass mode sets all the DAB to the maximum voltage, only the upper one is modulated to obtain the requested voltage. The first method is preferable for hi output power and the second gives advantages in low power working condition.

In conclusion, the design of electronic circuit for DEG management is complete. The choice of components and the definition of the control strategies is understood. A further step into implementation has been made. A prototype of one stage of the circuit was built and the preliminary debugging has been performed. The transformer is ready to be mounted. The inductance of the transformer has been measured respecting the expected theoretical values. The future work will be to build and debug the complete DAB circuit in order to define the exact module design and realize multiple copies of DAB modules.

2.3. Sensing

2.3.1. Sensing solutions

Figure 2-13 shows that charging and discharging of the DEG occurs when the capacitance is maximum and minimum respectively. This allows maximum exploitation of the membrane in terms of energy convertible per cycle. Several methods have been used to detect directly or indirectly the capacitance value. Indirect methods are based on external sensors that detect some parameter which is related to capacitance, for example the pressure inside the chamber in an OWC or the height of the tip of the membrane. To measure the tip elevation, a laser sensor can be used. However, this solution is not suitable for sea application because water spray can disturb the laser beam giving incorrect or faulty measurement. For this reason laser method has been used only in 'dry' lab test-bench application.

A more affordable solution is to measure the pressure, which is related to capacitance. The relation $C(p)$ is a monotonically increasing function. This means that when the capacitance is maximum, the pressure is also maximum. Thus, when the pressure derivative is zero also the capacitance derivative is zero. By just monitoring the pressure derivative, the controller can detect the proper instant to charge the DEG.

A direct way to measure the capacitance is to superimpose a small voltage sine wave to the high voltage of the DEG. Then, using a frequency domain analysis, the capacitance can be calculated in real-time. Using a superposed sine voltage whose frequency is much larger than typical sea waves allows the calculation of the capacitance on a time scale which is much shorter than the characteristic DEG deformation times, thus providing an accurate real-time estimate of the DEG capacitance.

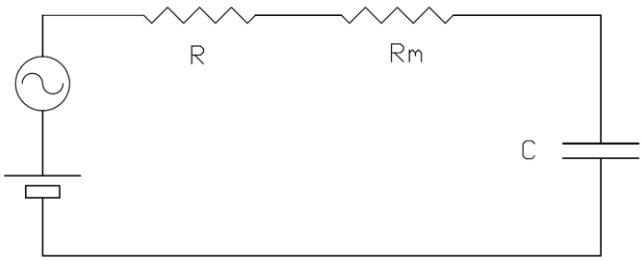

FIGURE 2-15: CIRCUIT FOR REAL TIME CAPACITANCE MEASUREMENT

The measurement of capacitance is performed applying a sinusoidal voltage to the CD-DEG (red wave in Figure 2-16). The voltage across a resistor in series to the DEG gives the measurement of the current (blue wave in Figure 2-16).

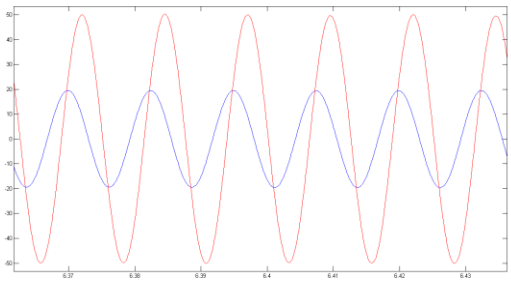

FIGURE 2-16: CAPACITANCE MEASUREMENT SIGNALS. THE RED LINE IS THE VOLTAGE (V), THE BLUE LINE IS THE CURRENT (MICROA).

The calculation of the capacitance is obtained measuring the amplitude and phase difference between the sine waves in real-time. The calculation of the amplitude comes immediately from maxima and minima detection, dividing their difference by two. The amplitude of the voltage is called V and the amplitude of current is called I. In order to calculate the phase (f) delay the product of the two sine waves is performed. The result of the product waveform will be called F:

$$F = V\sin(\omega t) I\sin(\omega t + \varphi) \tag{2.28}$$

The result of the product is:

$$F = \frac{VI}{2}(\cos(\varphi) - \cos(\omega t + \varphi)) \tag{2.29}$$

Applying a low-pass filter to F wave we get F':

$$F' = \frac{VI}{2}\cos(\varphi) \tag{2.30}$$

Reversing this formula the result is:

$$\varphi = acos\left(\frac{2}{VIF'}\right)\text{V} \tag{2.31}$$

At this point as shown in Figure 2-17 we know in real time the impedance phasor amplitude $|Z| = \frac{V}{I}$ and phase φ.

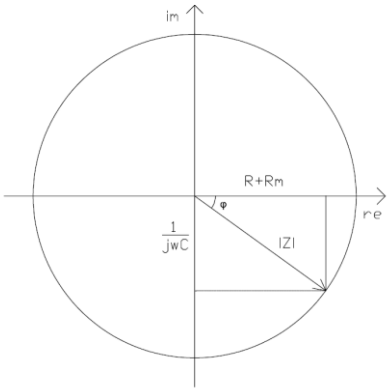

FIGURE 2-17: MEASUREMENT CIRCUIT IMPEDANCE PHASOR

The imaginary part of the phasor is the capacitive reactance:

$$X_c = \frac{1}{j\omega C_{DEG}} \tag{2.32}$$

Where C is the capacitance value we want to calculate. Putting all the equations together the expected result is:

$$C_{DEG} = \frac{1}{(\omega \cdot \sin(\varphi) \cdot |Z|)} \tag{2.33}$$

The value of the capacitance calculation of the DEG is performed in real-time and it's derivative gives the trigger to charge the DEG. The algorithm of calculation of the capacitance uses voltage and current measurement which are subjected to noise, this means that the real time capacitance readout can be affected by significant noise. Before calculating the derivative a filter must be applied to the capacitance signal. When the derivative is zero is the DEG charging or discharging time.

Any combination of the methods exposed above can be used to manage the DEG charging and discharging timing.

2.3.2. Self-sensing: experimental tests

An example of implementation of the capacitance direct measurement has been implemented in a lab test bench experiment session.

The circuit for capacitance measurement is shown in Figure 2-15. The voltage stimulus is provided by high voltage amplifier Trek 10/10B-HS. A sinewave with 80Hz frequency is superimposed to a DC voltage. The resistors are used to adjust the impedance seen from the voltage source. Since the measurement is based on the calculation of phase of the impedance the best condition for measuring impedance variations when the phase is near $-\frac{\pi}{4}$. Since the phase of the impedance is:

$$\varphi = \text{atan}\left(\frac{-\frac{1}{\omega C}}{R+R_m}\right) \tag{2.34}$$

The maximum variation of φ is calculated with the derivative $\frac{d\varphi}{dC}$. The maximum variation occurs when:

$$R + R_m = -\frac{1}{\omega C} \tag{2.35}$$

That corresponds to $= -\frac{\pi}{4}$. The reason why the resistors are two instead of one is related to the current measurement. The resistance calculated by equation (2.35) sets the angle φ. Then the current measurement is obtained from the voltage drop across the measuring resistor R_m. If the resistance is too high the voltage readout is too high for the measuring instrument input. In our case the instrument is Speedgoat Real Time Target which allows a maximum input signal of $\pm 10V$. The measure current amplitude is:

$$I = \frac{V}{|Z|} \tag{2.36}$$

Where:

$$|Z| = \sqrt{(R + R_m)^2 + \left(\frac{1}{\omega C}\right)^2} \tag{2.37}$$

The result is:

$$R_m = \frac{10V}{I} \tag{2.38}$$

The expected capacitance in our case is 7.9nF with undeformed membrane. From the equations above the values for the resistors are $R = 100k\Omega$ and $R_m = 1k\Omega$. The voltage amplitude is 100V.

The result of the experiment is shown in Figure 2-18. Here the membrane is deformed up to 65mm tip height and the voltage superimposed of 1000V.

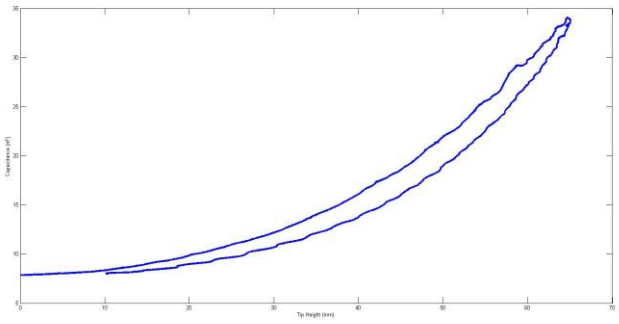

FIGURE 2-18: CAPACITANCE MEASURE PLOT

3. Control of submerged DEGs

3.1. Introduction

In this section, an approach for the study of the optimal control of a WEC based on DEG is proposed, that considers the fully-coupled WEC-DEG interaction dynamic problem and a model that represent the power system (with its limitations) that has been presented in the previous section.
The control techniques for DEG PTOs described in Section 1 (Figure 1-2) and in previous works on DEG PTOs rely on simple heuristics, e.g., the DEG is electrically charged when its capacitance reaches a maximum, it is then kept at a constant charge, or voltage, or maximum allowed electric field (compatibly with the failure conditions) as long as its capacitance decreases, and it is fully discharged when its capacitance hits a minimum. In effect, this type of control provides maximum converted energy density (per cycle) only if the DEG displacement is prescribed, and it is independent on the system dynamics.
In wave energy application, the DEG deformation results from a dynamic interaction between the DEG and a hydrodynamic interface. Changing the level of electrical loading (i.e., the maximum electric field) used in a cycle has a direct effect on the system oscillation amplitude itself (i.e., on the maximum DEG deformation), as the DEG damps the WEC dynamics and subtracts mechanical power from the primary hydrodynamic interface. Roughly, assuming a constant voltage control (Figure 1-2(b)), if an extremely high value of the maximum applied voltage was possible, its application would not necessarily result in a large converted power from the coupled WEC, as such a large electrical loading might provide an "overdamping" of the WEC itself, and consequent little deformations of the DEG PTO.
An appropriate controller for a WEC-DEG coupled system should thus perform one of the following alternative features:

- It controls the electrical state of the DEG (e.g., the voltage) in a cyclic way, based on a real-time optimization of the system dynamics, aimed at maximizing the WEC power output on a reference time horizon (on which a forecast of the wave excitation force is available).
- It relies on simple heuristics and on a finite sequence of prescribed electro-mechanical transformations (like the controllers in Figure 1-2), but includes control parameters that allow the regulation of the electrical loading level, based on the system dynamics and on the current sea state.

The implementation of both those control strategies require consideration of the coupled system dynamics and an optimization procedure on the average WEC power (over an observation time horizon). Rigorously speaking, the expression "optimum control" indicates the first of the two control strategies, while the second approach is simplified and aimed at achieving easier practical implementation of DEG PTOs control.

In the following, we first present a synthetic description of the techniques used to identify the optimum control aimed at maximizing the WEC power in presence of constraints due to the PTO.
Successively, we set our attention on a concept of Pressure Differential (PD) WEC, housing a DEG PTO in direct contact with sea water. We present a wave-to-wire model for the system, comprising modelling of the fluid-structure interaction between sea water and the DEG, and the electrostatic response of the DEG, included the electrical losses due to resistive electrodes and leakage currents (see Deliverable D 5.1). Due to the highly non-linear WEC response (due to both the complex fluid-structure interaction and to the electrical losses), the "optimum control" postulated before is very difficult to be mathematically identified and its real-time implementation is infeasible. We thus propose a simplified heuristic control strategy, which includes the possibility to regulate the level of electrical loading (with

respect to the maximum allowed electrical load) based on the current sea state and on long-term forecasts of the incident waves.

3.2. Optimum control

The behaviour of a typical WEC device usually depends on the dynamic parameters of the system: in order to achieve maximum energy extraction efficiency, the PTO mechanical impedance must be well adjusted. This condition can be easily expressed in a mathematical form using a frequency-domain representation of the system. The maximum useful absorbed energy for a body oscillating in one mode is achieved through the "complex conjugate control" [21].
Indicating by Z_{sys} the mechanical impedance of the WEC system, the optimal load impedance of the PTO has to equal the complex conjugate of the system impedance, Z_{sys}^{*}.
Complex-conjugate control holds provided that: 1) the system hydrodynamic response can be accurately modelled using a linear description (i.e., defining a mechanical impedance of the system), 2) there are no constraints on the WEC oscillation amplitude, on the PTO machinery force limits and on its dependence on the WEC displacement/velocity, 3) the PTO machinery is assumed ideal (there are no losses), which implies that the absorbed mechanical energy coincides with the harvested energy.
In the presence of constraints on the WEC oscillation amplitude or on the PTO force range, complex conjugate control does no longer provide an optimal solution. The problem of computing the maximum convertible power of a WEC subjected to constrained oscillations has been first tackled in [22]-[23] using a frequency-domain formulation. In practice, in presence of constraints on the maximum oscillation amplitude, the optimal control strategy is the "latching control" [21]. This strategy consists in latching the oscillating WEC in a fixed position during certain intervals of the oscillation cycle. The optimality of a latching-like control in the presence of oscillation amplitude constraints has been demonstrated in [9]-[11] using a time-domain approach.
DEG PTOs are generally subjected to constraints on both their oscillation amplitude (e.g., maximum deformation) and on the force range that they can provide in different configurations.
Controlling a DEG PTO in order to maximize the WEC power output in presence of known incoming waves is thus a constrained optimization problem. Recently, a methodology to compute optimal control cycles of a DEG PTO for OWC WECs has been studied in [12]. Such a methodology employs the formalism of Model Predictive Control (MPC) theory [13] and relies on a discretization of a prediction time horizon (e.g., a wave period, in the case of a monochromatic wave), and on the definition of discrete time-series for the relevant physical variables (e.g., WEC displacements and velocity, PTO force, etc.).
Discretizing and linearizing the dynamic equations, it is possible to formulate the power maximization problem as an optimization problem on a quadratic objective function (i.e., the average power generated by the WEC during the considered time horizon). The objective function can be properly provided with a set of constraints that account for the physical limitations and operating constraints of the DEG PTO. The solution of the constrained optimization problem provides the optimal control strategy for the DEG-based WEC (in the particular considered sea state). Mathematical details on this procedure are in [10] and [12].
Interestingly, such a mathematical procedure allows the consideration of a number of operational constraints, e.g., on the maximum instantaneous current and power supplied by the PTO. In [12], e.g., optimal control in presence of constraints on the maximum current provided by the DEG PTO is investigated.
In-line implementation of such an optimal control, i.e., real-time MPC on the DEG-WEC system, requires:

- Forecast of the incoming waves over a time horizon equalling the optimization time horizon. This can be achieved, e.g., with wave gauges located upstream of the WEC.

- A model of the system which allows to determine the state of the system (i.e., its dynamic variables) based on a restricted number of measured physical variables (e.g., the incoming waves profile, WEC velocities or displacements). The system model can be implemented, e.g., by augmented Kalman filters [10].
- A real-time solver for the constrained optimization problem, that outputs the optimal values of the control variable. With current computation capabilities, it seems that such a real-time solution can be obtained only if the control problem is formulated as a Quadratic Programming (QP) problem, with a quadratic objective function and linear constraints.

Due to the mentioned requirements, real-time implementation of a MPC strategy may result infeasible in practice, especially in DEG applications, because their non-linear response, as well as the complex relationships that quantify the electrical losses, usually make it difficult to express the power maximization problem as a QP problem.
Nonetheless, the mathematical solution of the optimization problem (in a set of sea states) found by using MPC-like formulations may provide qualitative indications to synthesise a real-time (prediction-free) controller, based on a finite sequence of electro-mechanical transformations, in the same fashion of the controllers of Figure 1-2.

3.3. Case study

In this section, we present a concept of generic Pressure Differential (PD) WEC equipped with a submerged DEG, which operates in direct contact with water and operates both as a PTO system and as a primary interface on which the wave excitation forces act.
After describing the device architecture and introducing a lumped-parameter numerical model for the complex hydro-electro-elastic interaction, we set the attention on the device control. Owing to the direct interaction between the waves and the polymeric stack and to the effect of electrical losses (which act as a penalization on the device power output), the resulting coupled model is non-linear. The problem of optimal PTO control (aimed at maximizing the power output while respecting the DEG operating constraints) is mathematically very complex, and cannot be directly tackled using the above-mentioned formalisms and MPC.
Therefore, we propose a real-time control strategy that allows the maximization of the power output based on long-term predictions of the wave climate (with no need for real-time forecast of the incoming waves). The theoretical control strategy is then combined with technological constraints on the maximum current and power that practical electronics can handle, and the effect of such limitations on the device dynamics and performance are evaluated.

3.3.1. Concept description

The proposed PD DEG-WEC is based on a simple axial-symmetric shape, shown in Figure 3-1. The device is hereafter referred to as DrumWEC, and it consists in a DE membrane (or stack of membranes) the faces of which are covered by compliant electrodes, that acts as PTO system. The DE membrane is referred to as Immersed Circular Diaphragm DEG (ICD-DEG). The ICD-DEG is mounted (with a certain amount of pre-stretch) on top of a submerged air chamber, it contacts air with its bottom face, and sea water and incoming waves with the upper face. In the absence of electric activation, the DE membrane behaves as a passive elastic component, and it is deformed by the action of sea waves, i.e., the larger the excitation loads and/or overlying water head, the greater downward membrane deformations (membrane deflection is schematised in Figure 3-1).
Membrane deformations are responsible for electric capacitance variations. By properly controlling the electric activation of the DE PTO, capacitance variations can be exploited to convert mechanical energy from the waves into electric energy (according to the principle illustrated in Figure 1).

The DEG PTO is eventually surrounded by a collector with the aim of taking the inlet section closer to the sea surface (thus increasing the wave excitation), canalizing the flux, and increasing the inertia of the device.

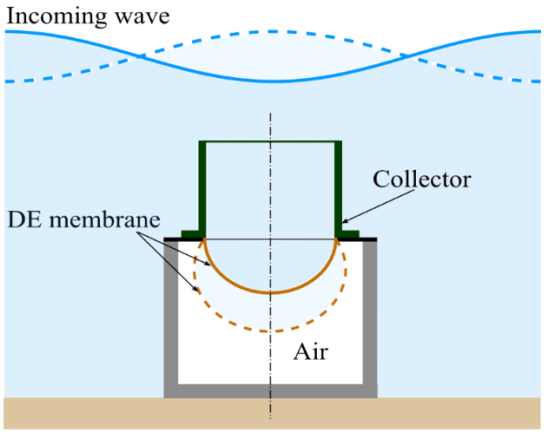

FIGURE 3-1: SCHEMATIC REPRESENTATION OF THE DRUMWEC OPERATING PRINCIPLE.

The dynamics of the device is dominated by the elastic response of the membrane (spring effect) and by the fluid added mass, given that the mass of the membrane can be neglected.
The air volume within the submerged tank also participates to DrumWEC dynamics by adding a further stiffness that sums up to hydrostatic and membrane stiffness.
In contrast to other concepts of DEG-based WEC, DrumWEC has the interesting feature of combining positive DEG mechanical stiffness with negative hydrostatic stiffness. Indeed, a downward deformation of the DEG corresponds to an increase in the elastic restoring force of the DEG itself and an increase in the downward-pushing hydrostatic pressure of the surrounding water.
The need for DEG stiffness compensation through increased added mass (present, for example in OWCs with DEG PTO) does not apply to this device. Intrinsic stiffness compensation can be exploited to design WECs with the following alternative features:

- PD WECs which have nearly-zero total stiffness, and respond with large deformations to waves with relatively modest amplitude.
- PD WECs whose stiffness is chosen, by design, to achieve resonance. As stiffness compensation can be virtually achieved at any scale, resonating devices with modest dimensions can be potentially designed.

A further method for modifying/adjusting the dynamic response of the system consists in regulating the average pressure inside the air chamber. For a given depth, the pressure could be increased in order to reduce the membrane downward deformation, and vice versa decreased to make it further expand downward. This can have an influence on the stiffness of the system, since the elastic response is strongly non-linear and stiffness is variable with the amplitude of deformation. However, this feature is only achieved by introducing an air-pressure regulator that would significantly increase the complexity of the system.
In this section, we provide a detailed description of the hypothesis and governing equations of the DrumWEC dynamics. For our current aims of preliminary design and control specifications definitions, and in order to show the sensitivity of the model to different parameters, we keep the model as much "analytical" as possible, i.e., we employ simplifying assumptions and assume that the deformation kinematics of the ICD-DEG is described by one Degree-of-Freedom (DoF). Despite this simplification, we take into account non-linear terms as non-linear Froude-Krylov excitation forces and second order

hydrodynamic terms, and we employ a non-linear electro-elastic model for the DEG, whose response is preliminarily mapped via FEM.

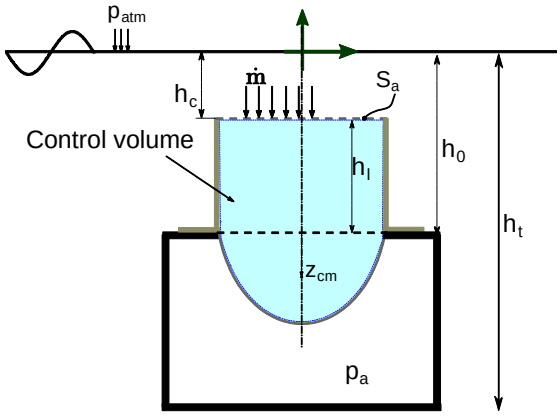

FIGURE 3-2: DEFINITION OF DRUMWEC DIMENSIONS AND CONTROL VOLUME (SHADOWED AREA).

3.3.1.1 HYDRODYNAMIC AND FLUID-STRUCTURE INTERACTION MODEL

Figure 3-2 introduces the main variables used in the analytical hydrodynamic model of the DrumWEC. We consider a DrumWEC prototype provided with an upper collector of cylindrical shape on top of the ICD-DEG PTO, as shown in Figure 3-2. We define a control volume, constituted by the water volume included among the top section of the collector and the ICD-DEG. The control volume is open, as water can flow through the (fixed) collector upper section, and deformable because of the ICD-DEG movement. The system has one DoF, and we choose the volume Ω_c comprised between the ICD-DEG upper surface and the horizontal plane holding the DEG perimeter as a generalized variable for the problem (i.e., the position of the ICD-DEG is uniquely identified by Ω_c).

The following physical quantities are introduced:

- ρ is water density;
- g is gravity acceleration;
- h_0 is the depth of the membrane base-plane (i.e., the plane housing the membrane perimeter);
- p_a is the absolute air pressure in the submerged chamber;
- S_a is the collector inlet section area;
- $\dot{m}$ is the mass flow rate trough S_a (positive if water enters);
- z_{cm} is the vertical distance of the water cap centre of mass from the membrane base-plane (in the reference frame shown in Figure 3-2);
- Ω_a is the volume of the air chamber in a generic configuration.

Owing to water incompressibility, water velocity at the inlet section (assumed uniform) is $v = \dot{\Omega}_c / S_a$, and $\dot{m} = \rho \dot{\Omega}_c$.
The global energy balance for the reference control volume is as follows:

$$\frac{d}{dt}\left(E_k + E_g + E_{el} + E_{es}\right) = \dot{W}_v + \dot{W}_{es} + \dot{W}_a + \dot{W}_{in} \qquad (4.1)$$

where:

- E_k is the kinetic energy of water within the control volume. Using velocity $\dot{h}$, kinetic energy has the following quadratic form:

$$E_k = \frac{1}{2}\rho S_a h_l v^2 + \frac{1}{2}\rho \Omega_c \dot{z}_{cm}^2 = \frac{1}{2}\rho h_l \frac{\dot{\Omega}_c^{\,2}}{S_a} + \frac{1}{2}\rho \Omega_c \dot{z}_{cm}^2 \tag{4.2}$$

where z_{cm} depends on Ω_c. For simplicity, the kinetic energy due to the displacing water cap has been approximated to the kinetic energy of a rigid body with volume Ω_c and linear velocity $\dot{z}_{cm}$, and the contribution due to relative velocity of the water particles with respect to the centre of mass (whose knowledge would require exact solution of the water flow distribution) has been neglected.

- E_g is the potential gravitational energy of the water within the control volume. Using the still water level as set point for the potential energy (i.e., potential energy is zero on that plane), E_g reads as:

$$E_g = E_{g,col} + \rho g \Omega_c z_{cm} \tag{4.3}$$

where $E_{g,col}$ is a constant and it stands for the potential energy of the (fixed) water volume comprised in the control volume above the membrane perimeter plane, while the second addendum is the potential energy of the water cap under the membrane perimeter plane.

- E_{el} is the elastic energy of the membrane in the considered configuration, and it is a function solely of Ω_c.

- E_{es} is the electrostatic energy stored in the DEG, given by

$$E_{es} = \frac{1}{2} C V^2 \tag{4.4}$$

where V is the voltage on the DEG electrodes, and C its capacitance, depending only on h.

- W_v is the power dissipated by the hydrodynamic viscous forces. It can be expressed as a function of the water volume flow rate, $\dot{\Omega}_c$, with reference to the dynamic pressure at the inlet section, as follows:

$$\dot{W}_v = -\dot{\Omega}_c \frac{1}{2}\rho |v| v = -\frac{K_v}{2}\frac{\rho}{S_a^2}\left|\dot{\Omega}_c\right|\dot{\Omega}_c^2 \tag{4.5}$$

where K_v is a viscous coefficient (usually in the order of magnitude of the unity).

- $\dot{W}_{es}$ is the electrostatic energy supplied to the system (namely, the DEG), by the external power electronics (positive if supplied from the exterior to the DEG):

$$\dot{W}_{es} = V\dot{Q} = V^2\dot{C} + Q\dot{V} \tag{4.6}$$

being $Q = CV$ the instant charge on the DEG electrodes.

- $\dot{W}_a$ is the power associated to the mechanical work done by air (in the submerged chamber) on the control volume:

$$\dot{W}_a = -p_a \dot{\Omega}_c \tag{4.7}$$

It can be assumed that air in the chamber evolves adiabatically:

$$p_a \Omega_a^{\gamma} = p_{a,0} \Omega_{a,0}^{\gamma} \tag{4.8}$$

where $p_{a,0}$ and $\Omega_{a,0}$ are absolute air pressure and chamber volume in the static equilibrium configuration, and γ=1.4 is the adiabatic air ratio and

- $\dot{W}_{in}$ is the power entering the system through the inlet section S_a. It is composed by the following terms: pressure (atmospheric pressure + hydrostatic pressure + wave induced pressure, p_w) insisting on S_a, kinetic energy density, and potential energy density of the water flowing through S_a:

$$\dot{W}_{in} = \dot{\Omega}_c \left[(p_{atm} + \rho g h_c + p_w) + \rho \frac{v^2}{2} - \rho g h_c \right] = \dot{\Omega}_c \left[p_{atm} + p_{exc} + p_{rad} + \frac{1}{2} \rho \frac{\dot{\Omega}_c^2}{S_a^2} \right] \quad (4.9)$$

where p_w has been split into two addenda: one owing to wave excitation force, the other owing to radiated waves.

Mean excitation and radiation wave pressures on S_a can be defined as follows, by introducing excitation and radiation potentials (ϕ_{exc} and ϕ_{rad}) [1]:

$$p_{exc} = \frac{\rho}{S_a} \int_{S_a} \frac{\partial \phi_{exc}}{\partial t}; \quad p_{rad} = \frac{\rho}{S_a} \int_{S_a} \frac{\partial \phi_{rad}}{\partial t} \quad (4.10)$$

The following assumptions have been used:
1) The kinetic and gravitational energy of the membrane are negligible with respect to those of water;
2) The DEG has ideal behavior, i.e., no electro-viscoelastic dissipations are considered in the balance equation. Indeed, ICD-DEG capacitance has assumed to be equivalent to that of planar capacitor with variable thickness;
Substituting equations (1)-(10) into energy balance equation (1) and dividing by $\dot{\Omega}_c$, the following dynamic equation is found:

$$M(\Omega_c)\ddot{\Omega}_c + \frac{1}{2} M'^{(\Omega_c)} \dot{\Omega}_c^2 - \frac{1}{2} \frac{\rho}{S_a^2} \dot{\Omega}_c^2 + \rho g (z_{cm} + \Omega_c z'_{cm}) + E'_{el} = -\frac{K_v}{2} \frac{\rho}{S_a^2} |\dot{\Omega}_c| \dot{\Omega}_c + \frac{V^2}{2} C' - p_a + p_{atm} + p_{exc} + p_{rad} \quad (4.11)$$

where $M(\Omega_c) = \frac{\rho h_l}{S_a} + \rho\, \Omega_c (z'_{cm})^2$ is a generalized inertia and the prime superscript stands for the derivative with respect to Ω_c. Time derivatives of M, z_{cm}, E_{el} and C have been expressed as the product of derivative with respect to Ω_c times $\dot{\Omega}_c$. A generalised static force can be introduced:

$$F_{h,st}(\Omega_c) = -\rho g (z_{cm} + \Omega_c z'_{cm}) - E'_{el} \quad (4.12)$$

Calculation of p_{exc} and p_{rad} is non-trivial, as it requires a solution for wave excitation and radiation potentials (equation (10)). Radiation potential, in particular, is a memory term which depends on the previous history of the system.

In practice, it is expected that the DrumWEC collector will be much smaller than the wavelength, and it will behave as a point absorber. The excitation pressure can be thus approximated to the sole Froude-Krylov contribution neglecting the diffraction component, as stated in [2]. Averaging the expression of the pressure due to an undisturbed linear wave (regular wave with height H and angular frequency ω) [3] over the collector inlet section, and substituting the result to p_{exc} yields to the following expression for the excitation force:

$$p_{exc}(t) = \frac{\rho g H}{2} \Im(\omega) \frac{\cosh(k_w (h_w - h_c))}{\cosh(k_w h_w)} \cos(\omega t) \quad (4.13)$$

where h_w is the water depth, k_w is the wave number (related to the water depth and to the wave frequency through well-known relationships [3]), and factor $\Im(\omega)$ comes from an integration on the inlet section and reads as follows:

$$\Im(\omega) = \frac{4}{S_a} \int_0^{\pi/2} \int_0^{r_a} \xi \cos(k_w \xi \cos\theta)\, d\xi\, d\theta \quad (4.14)$$

where r_a is the radius of the collector inner section ($S_a = \pi r_a^2$).

In the practical case of real sea waves, the excitation pressure time-series can be approximated to a finite sum of harmonic contributions as follows:

$$p_{exc}(t) = \sum_{i=1}^{n} A_{w,i}\Gamma(\omega_i)\cos(\omega_i t + \varphi_i), \tag{4.15}$$

where $\Gamma(\omega)$, that is the wave excitation coefficient, can be deduced from equation (13):

$$\Gamma(\omega) = \rho g \Im(\omega) \frac{\cosh(k_w(h_w - h_c))}{\cosh(k_w h_w)}, \tag{4.16}$$

φ_i are random phases between 0 and 2π, and $A_{w,i}$ are the wave amplitudes of the various regular wave components, given by:

$$A_{w,i} = \sqrt{2\Delta f_i S_f(f_i)}, \tag{4.17}$$

where Δf_i is the difference between (i+1)-th and i-th frequencies $f = \omega/(2\pi)$, and $S_f(f)$ is the spectral power density depending on the wave parameters (i.e., significant wave height, H_s, and peak period, T_p).

Following a common practice in wave energy literature, radiation force can be linearized and reduced to the following form:

$$F_{rad} \approx \int_0^t k(t-\tau)\dot{\Omega}_c(\tau)d\tau \tag{4.18}$$

where we have introduced a radiation convolution kernel, $k(t)$, which is the inverse Fourier transform of the (frequency-domain) radiation impedance function:

$$K(\omega) = B_r(\omega) + i\omega M_{ad}(\omega) \tag{4.19}$$

where $B_r(\omega)$ and $M_{ad}(\omega)$ are, respectively, the radiation damping and the fluctuating (frequency-dependent) component of the added mass. Owing to the device axial symmetry, such coefficients can be calculated from $\Gamma(\omega)$ using Haskind and Kramers relations:

$$B_r(\omega) = \frac{\omega k_w \Gamma^2(\omega)}{2\rho g^2 \Upsilon}, \quad \text{with} \quad \Upsilon = \left[1 + \frac{2k_w h_w}{\sinh(2k_w h_w)}\right]\tanh(k_w h_w)$$
$$M_{ad}(\omega) = -\frac{2}{\pi}\int_0^\infty \frac{B_r(\xi)}{\omega^2 - \xi^2}d\xi \tag{4.20}$$

3.3.1.2 DEG MODEL

A DEG static model is required to map the ICD-DEG elastic energy, E_{el}, the centre of mass position of the water cap, z_{cm}, and the DEG capacitance, C, as functions of Ω_c. ICD-DEG continuum equations are presented in the following.

An ICD-DEG is depicted in Figure 3-3. It consists of an equi-biaxially pre-stretched planar circular DE Membrane (DEM) that is clamped along its perimeter at radius e and with thickness t (whereas e_0 and t_0 indicate the radius and thickness of the DEM in its planar undeformed state). We designate the radial pre-stretch as λ_p $\left(\lambda_p = e/e_0\right)$. Assuming the DE material as incompressible [4], the thickness t in the flat stretched configuration is $t = t_0/\lambda_p^2$.

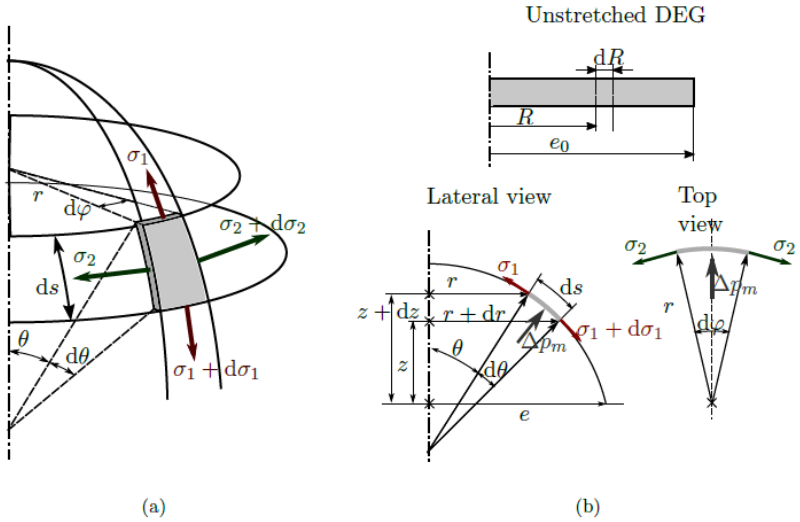

FIGURE 3-3: (A) INFLATED I-DEG INFINITESIMAL ELEMENT AND APPLIED STRESSES. (B) DEFINITION OF COORDINATE R IN THE UNSTRETCHED CONFIGURATION (TOP); LATERAL AND TOP VIEW OF THE INFINITESIMAL ELEMENT IN THE INFLATED CONFIGURATION.

When the opposing faces of the ICD-DEG are subjected to a differential pressure and to voltage, the ICD-DEG undergoes an out of plane axial-symmetric (bubble-like) deformation (area expansion). In Figure 3-3 (b), h identifies the resultant displacement of the ICD-DEG tip.

Similarly to [4], we treat the generic ICD-DEG as a thin shell, and we consider the mechanical equilibrium of an infinitesimal portion of material, as shown in Figure 3-3

We indicate with R the distance of the infinitesimal element from the axis in the unstretched configuration (Figure 3-3 (b)). After deformation (pre-stretch + inflation), the element lies at a distance r (measured on the horizontal plane) from the axis and at distance z from the plane housing the DEG perimeter (see Figure 3-3 (b)).

Due to axial symmetry, the principal stretches [4] are meridian, circumferential, and in thickness direction, and they reads as follows:

$$\lambda_1 = \frac{\mathrm{d}s}{\mathrm{d}R} = \sqrt{\left(\frac{\mathrm{d}r}{\mathrm{d}R}\right)^2 + \left(\frac{\mathrm{d}z}{\mathrm{d}R}\right)^2} \quad ; \quad \lambda_2 = \frac{r}{R} \quad ; \quad \lambda_3 = (\lambda_1\lambda_2)^{-1} \tag{4.21}$$

where the differential length ds is defined in Figure 3-3 (b), and the third equation owes to DE material incompressibility, i.e., the local membrane thickness equals $t_0/(\lambda_1\lambda_2)$.

Indicating with Δp_m the local pressure difference between the membrane faces, equilibrium condition of the element in the horizontal and vertical directions leads to the following equations:

$$\begin{aligned} \frac{d}{dR}\left(\frac{\sigma_1 R}{\lambda_1^2}\frac{\mathrm{d}r}{\mathrm{d}R}\right) &= \frac{\Delta p_m R\,\lambda_2}{t_0}\frac{\mathrm{d}z}{\mathrm{d}R} + \frac{\sigma_2}{\lambda_2} \\ \frac{d}{dR}\left(\frac{\sigma_1 R}{\lambda_1^2}\frac{\mathrm{d}z}{\mathrm{d}R}\right) &= -\frac{\Delta p_m R\,\lambda_2}{t_0}\frac{\mathrm{d}r}{\mathrm{d}R} \end{aligned} \tag{4.22}$$

where σ_1 and σ_2 are the principal stresses. The following boundary conditions apply:

$$r(0) = 0,\ r(e_0) = e,\ \left(\frac{\mathrm{d}z}{\mathrm{d}R}\right)_0 = 0,\ z(e_0) = 0 \tag{4.23}$$

Following a consolidated approach employed in rubber mechanics [5], the DE membrane is treated as an incompressible hyperelastic solid, i.e., a constitutive model is used which relates elastic energy density (namely, strain energy function, Ψ) to the principal stretches λ_1 and λ_2:

$$\Psi = \Psi(\lambda_1, \lambda_2) \tag{4.24}$$

Several constitutive models exist [6], which provide an analytic form for equation (24) and allow to compute the principal stresses as follows:

$$\sigma_1 = \lambda_1 \frac{\partial \Psi(\lambda_1,\lambda_2)}{\partial \lambda_1}, \quad \sigma_2 = \lambda_2 \frac{\partial \Psi(\lambda_1,\lambda_2)}{\partial \lambda_2} \tag{4.25}$$

In the present application, Δp_m in equations (22) is the local pressure difference between the water (on the upper DEG face) and the air (on the lower face). With reference to FIGURE 3-2, in a static equilibrium configuration where the absolute air pressure equals p_a, Δp_m reads as follows:

$$\Delta p_m = \rho g(z - h_0) + p_a - p_{atm} \tag{4.26}$$

Replacing the terms in equations (25)-(26) into equation (22), solutions for $r(R)$ and $z(R)$ in the static equilibrium configuration are found.

In general, the deformed ICD-DEG shapes in static conditions can be mapped by setting $\Delta p_m = \rho g(z - h_c)$, and solving equations (22) at different values of h_c. This corresponds to a scenario in which the air gauge pressure in the chamber is null and different water column heights, h_c, on the membrane perimeter are considered.

Doing this, it is possible to map E_{el}, z_{cm}, C, and Ω_c, as a function of h_c. In particular, the mentioned quantities can be calculated using the solutions for $r(R)$ and $z(R)$ as follows:

$$\Omega_c = -\int_{\Omega_c} \pi r^2 \, \mathrm{d}z\,, \; z_{cm} = \frac{\int 2\pi r z dz}{\Omega_c}\,, \; E_{el} = \int_0^{e_0} 2\pi t_0 R \Psi(\lambda_1,\lambda_2)\mathrm{d}R\,, \; C = 2\pi\varepsilon n_L^2 \int \frac{r\lambda_1\lambda_2 \, \mathrm{d}s}{t_0} \tag{4.27}$$

where ε is the DE dielectric constant, n_L is the number of DE layers (electrically in-parallel) in the stack, which only affects the capacitance, and can be chosen on the basis of electrical requirements of the system, e.g., the maximum admissible output voltage.

Using those expressions, it is possible to express E_{el} and C as functions of Ω_c.

With reference to the DrumWEC operation, we hereby assume that the deformed shapes identified by such a static calculation fully define the ICD-DEG kinematics, even in operating conditions different from the static conditions. Therefore, the mapped values of E_{el}, z_{cm} and C can be directly fed into dynamic equation (11). In practice, equation (22) can be solved numerically (using a boundary-value problems solver, like COMSOL Multiphysics®) by considering a finite set of water heads, h_c, above the membrane perimeter. Relevant quantities as functions of Ω_c are obtained by interpolation.

As regards the electrical losses, they are not directly included in the energy balance of equation (1). In fact, their contribution to the system dynamics is considered negligible, and their effect can be taken into account "a posteriori", by calculating the electrical power dissipated due to the electrodes and the DE material conductivity and subtracting it from the electrical power calculated in the absence of electrical losses.

With reference to the ICD-DEG topology, numerical models to calculate the power dissipated owing to the DE conductivity and the power dissipated during DEG charging/discharging due to the compliant electrodes are widely described in Deliverable D5.1.

3.3.1.3 AIR MODEL

We denote by p_0 the absolute air pressure in the static equilibrium configuration (i.e., in the absence of waves). The corresponding equilibrium configuration for the ICD-DEG (among those obtained at different h_c values as described before) is that identified by $h_c = h_0 - (p_0 - p_{atm})/(\rho g)$.

During operation, the air volume is closed, and no air can flow in or out of the chamber. Assuming that air undergoes iso-entropic transformations, the following relation holds:

$$p_a \Omega_a^\gamma = p_0 \Omega_{a,0}^\gamma \tag{4.28}$$

where $\Omega_{a,0}$ and Ω_a are the air volumes in the static equilibrium configuration (in presence of pressure p_0).

3.3.2. Control

This section deals with control laws for the ICD-DEG PTO.

A simple control strategy based on the ICD-DEG physical limits is presented. The chosen control does not require any prediction of the incoming waves, and it only relies on the instantaneous membrane physical state.

The ICD-DEG capacitance decreases as it moves toward the flat horizontal position (i.e., upward motion if the DEG deformed shell lies below the horizontal plane). Following a common practice in DEG PTOs literature [7]-[8], a simple control strategy consists in keeping the DEG electrically active only when its capacitance decreases, and setting its voltage to zero as its capacitance is increasing. Triggering between successive phases (in the absence or presence of electric activation) can be achieved based on real-time measurements of one or more sensor, e.g., directly measuring the ICD-DEG capacitance (compatibly with the power electronics circuit), measuring the membrane deformation (e.g., the position of its tip), or the air pressure within the submerged chamber (maxima in such a pressure correspond to maxima in the ICD-DEG deformation and capacitance).

As regards the level of electrical loading (voltage) to be kept on the ICD-DEG during the electrically active phases, in [8], for the case of an OWC with DEG diaphragm PTO, it was suggested to activate the DEG at the maximum allowed electric field (compatibly with constraints) whenever the controller requires it to be electrically active.

In DrumWEC application, however, that control strategy may result over-aggressive, because it would keep the ICD-DEG still in some downward expanded position. Therefore, we hereby assume that, during activation, the electric field at the ICD-DEG tip is a prescribed share, β (with $0 < \beta \leq 1$), of the break-down field, E_{BD} (which is a material property of the considered DE and of the material stretch). The operating constraints of the ICD-DEG (maximum/minimum capacitance, electrical break-down) and an example of conversions cycle are shown in Figure 3-4, on a plane whose axes represent the DEG charge and voltage. In the picture, the conversion cycle is indicated by the closed loop OABO, where OA represents instant charging of the DEG (which takes place when the DEG is in a specific configuration, the capacitance of which is identified by the slope of line OA), AB is the active generation phase (the DEG capacitance decreases, and electric field is kept at a share β of E_{BD}), BO is the instant discharging phase (BO is an iso-capacitance line representing the minimum capacitance hit by the DEG in the cycle under investigation).

We can assume that β is changed throughout the different sea states, and numerically optimized for each sea state in order to maximize the power output. Varying β at each sea state does not imply an in-line prediction of the incoming wave, as this is chosen to be a long-term adjustment that can be performed basing on occasional wave climate forecasts. Optimal values of β at the different sea states can be mapped basing on numerical simulations.

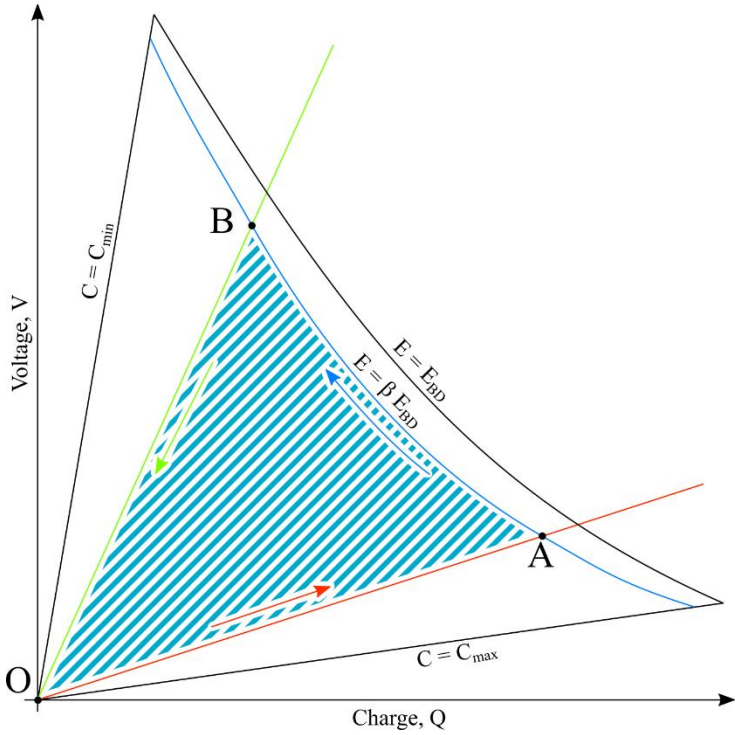

FIGURE 3-4 EXAMPLE OF ENERGY CONVERSION CYCLE FOR A DEG ON THE *Q-V* PLANE.

The simple control strategy proposed in the previous paragraph does not provide the absolute optimum solution envisaged in Sect. 3.2.

In general, optimal control (that maximizes the produced power) might require a more complicated control pattern to be pursued. With reference to the charge-voltage plane representation provided in Figure 3-4 about the previous control, the optimal control cycle would result in a complex closed loop bounded by the operating constraints, and generally different from cycle OABO.

Interestingly, in [12] it is shown that, for an OWC equipped with a circular diaphragm DEG with given features, an optimal control strategy was deduced, which is similar to that described in the previous Section and in Figure 3-4, in particular:

- β should be set to 1 in all the different sea states,
- DEG charging/discharging is delayed or anticipated with respect to the time instants in which the DEG capacitance reaches maximum/minimum values, depending on the specific sea states.

3.3.3. Engineering constraints

The maximum electric field that a DE material can stand (namely, the break-down electric field) generally depends on the applied stretch as follows:

$$E_{BD} = E_{BD,0}\lambda_3^{-R_e/2}, \quad (4.29)$$

where $E_{BD,0}$ and R_e are material parameters and λ_3 is the local stretch in the DE layers thickness direction (as opposed to λ_1 and λ_2, that are the principal stretches tangential to the DE layers surface).

With reference to the ICD-DEG, being V the voltage applied on its electrodes, the electric field on a generic point of the DEG results in

$$E = V/(t_0 n_L \lambda_3). \quad (30)$$

Setting $E \leq E_{BD}$ results in a limitation on the voltage:

$$V \leq E_{BD,0} t_0 n_L \lambda_3^{1-R_e/2}, \quad (31)$$

As (31) must hold in any point of the ICD-DEG, the maximum allowed voltage is set by the minimum value of $\lambda_3^{1-R_e/2}$. In practical DE materials, R_e is lower than 2 [14]. Therefore, $\lambda_3^{1-R_e/2}$ is minimum at the DEG tip, where the membrane is stretched equibiaxially and its thickness is minimum. The break-down condition can be thus formulated as a condition on the maximum electric field at the DEG tip only, without losing generality.

To manage consistent electric energy density, DEGs need to be operated at electric fields in the same order of the break-down field (hundreds of MV/m), meaning that their peak output voltage (at the scale of wave energy PTOs application) is in the order of tens of kV. This choice represents a compromise between excessive voltages (which would make the power electronics more complicated and the wires for transportation more expensive) and an excessive number of DE layers that would be required to further reduce the peak voltage at the same applied electric field.

With reference to the ICD-DEG PTO, the number of layers can be chosen as follows. Owing to the control described in the previous section and in Figure 3-4, the DEG reaches maximum voltage when its capacitance is minimum. The minimum feasible value for the ICD-DEG capacitance is reached in the flat horizontal configuration. In such a configuration, the ICD-DEG features break-down electric field of $E = E_{BD,0}\lambda_p^{R_e}$ (where λ_p is the pre-stretch). As the ICD-DEG has thickness of $t = t_0\lambda_p^{-2}$ in the flat pre-stretched configuration (notice that this is the thickness of DE only, neglecting electrodes thickness), in order to limit the DEG output voltage to a certain value, V_{max}, at least $n_L = \frac{E_{BD,0}t_0}{\lambda_p^{2-R_e}V_{\max}}$ layers are required.

Another engineering constraint involved in the ICD-DEG operation regards the maximum current and power supplied by/to the DEG during the discharging/charging phases (e.g., phases BO and OA in Figure 3-4). According to the control strategy described in the previous section, charging and discharging of the ICD-DEG are instantaneous, and they are triggered by maxima/minima in the capacitance time-series. In effect, instantaneous charge variations would result in infinite (impulsive) current and power flowing in/out of the DEG. However, this condition is not practically feasible due to 1) limitations of the electric machinery (i.e., the DC-DC converter supplying/harvesting energy to/from the DEG) and rated power/currents of its components (in particular, the switching semiconductor components); 2) electric losses that would arise due to electrodes resistivity if infinite currents are applied on the electrodes. In practice, it is required to limit the maximum module of current and power applied on the DEG. This results in non-instantaneous charging/discharging operations.

Indicating with I_{max} and P_{max} the maximum acceptable current and power supplied to/by the DEG (in module), the control logics (regulating the current supplied to the DEG) can be coded as follows:

```
% Activation triggering
if(Ck<Ck-1)
    act=1;
else
    act=0;
end

% Values of the electric variables (at instant k) if no current/power
% limitations were present
Ek=act*EBD,0*λ3,k^-Re/2 ; % electric field
Vk=β*Ek*t0*λ3,k/nL;     % voltage
Qk=Vk*Ck; % charge
```

```
% Limiting the current value in the light of current/power constraints
Ik=sign(Qk-Qk-1)*min{|Qk-Qk-1|/Ts, Imax, Pmax/Vk-1};
```

where

- A discrete controller with a sample time T_s has been assumed. Index *k* indicates the *k*-th time instant;
- E_k, V_k, Q_k are auxiliary variables indicating the "desired" electric field (at the ICD-DEG tip), voltage and charge at the *k*-th time instant (in case no current/power constraints were present).
- I_k is the commanded current at the the *k*-th time instant (positive if supplied to the DEG);
- β is the electric field's partialization coefficient (as defined in previous sections);
- the values of capacitance and stretch (in the thickness direction) at the various instants (C_k, $\lambda_{3,k}$) are known (by direct measurement or by estimates from directly measured variables)

3.3.4. Case study

In this section, we present a numerical case study of a DrumWEC device with given dimensions. The system features a design that benefits from the mutual hydrostatic and elastic loads compensation, therefore it features low total rigidity over a wide range of deformation.
The device features a cylindrical air chamber collector with the properties listed in Table 3-1 (a). The ICD-DEG is made of a styrene-based rubber (properties are in Table 3-1 (b) [15]), and its geometric features are inTable 3-1 (c). The proposed design features a relatively large air chamber compared to the ICD-DEG diameter, to provide a sufficiently large air volume and limit the stiffness of the air.
The parameters involved in the computation of electrical losses are in Table 3-1 (b).

Air chamber diameter	15 m
Air chamber height	11 m
Collector Radius, r_a	4 m
Collector height, h_l	4.5 m
Membrane perim. depth, h_0	9 m
Air chamber Volume, $\Omega_{a,0}$	1940 m³

(a)

Hyperelastic model (generalized Mooney-Rivlin model): $\Psi = \sum_{i=1}^{3} A_i(I_1-3)^i + \sum_{j=1}^{2} B_j(I_2-3)^j$ $I_1 = \lambda_1^2+\lambda_2^2+\lambda_1^{-2}\lambda_2^{-2}$; $I_2 = \lambda_1^{-2}+\lambda_2^{-2}+\lambda_1^2\lambda_2^2$	A_1=1.03 MPa; A_2=0.17 MPa; A_3=-4.11 kPa; B_1=-0.59 MPa; B_2=1.84 kPa;
Break-down electric field	$E_{BD,0}$ =97.27MV/m, R_e=1
Dielectric constant	E=2.7×8.85e-12 F/m
DE conductivity, $\kappa=\kappa_0\exp(E/E_0)$	κ_0=6.4e-15 S/m E_0=56 MV/m
Electrode sheet resistance	R_s=345 Ω/□

(b)

DEG stretched radius, e	4 m
DEG pre-stretched thickness, *t*	8 cm
Pre-stretch	1.6

(c)

TABLE 3-1 (A) FEATURES OF THE DRUMWEC COLLECTOR AND SUBMERGED AIR CHAMBER (B) PHYSICAL PROPERTIES OF THE REFERENCE DE MATERIAL (STYRENE-BASED RUBBER [15]); (C) FEATURES OF THE REFERENCE ICD-DEG.

3.3.4.1 FEM MODEL OF THE PTO

The computation of the static ICD-DEG response has been carried out using the "thin shell" solver of the Structural Mechanics Module of the commercial FEM software COMSOL Multiphysics®.

To determine the static mechanical response, the ICD-DEG has been modelled as a monolithic thick DE layer (electrodes thickness is neglected), subjected to axisymmetric deformation. The static analysis has been carried out by progressively increasing the water head on top of the membrane edge, h_C (assuming null gauge pressure on the lower face). The water column pressure has been prescribed as an implicit pressure boundary condition on the ICD-DEG upper face, depending on the local vertical displacement of the DEG face.

Constant increments of h_C have been considered, and the corresponding membrane deformed shapes have been found.

Figure 3-5 shows the ICD-DEG deformed shape in correspondence of constant h_C increments. The picture shows that a deformation range exists in which the membrane tends to become softer and undergoes larger deformations. This is the result of positive elastic stiffness and negative hydrostatic stiffness mutual cancellation.

FEM data are used to identify the DEG static equilibrium position. In particular, denoting by h_0 and p_0 the actual water head above the membrane perimeter and the air pressure at equilibrium, the reference equilibrium shape corresponds to $h_C = d_0 - (p_0 - p_{atm})/(\rho_w g)$. The equilibrium shape in Figure 3-5 is achieved with gauge air pressure of 54 kPa, and membrane perimeter depth of 9 m.

Membrane shape, elastic energy, capacitance and the other static quantities in equation (11) are mapped with respect to the volume Ω_c subtended by the DEG as explained above. Those quantities are required to identify the system static response, given by equation (12).

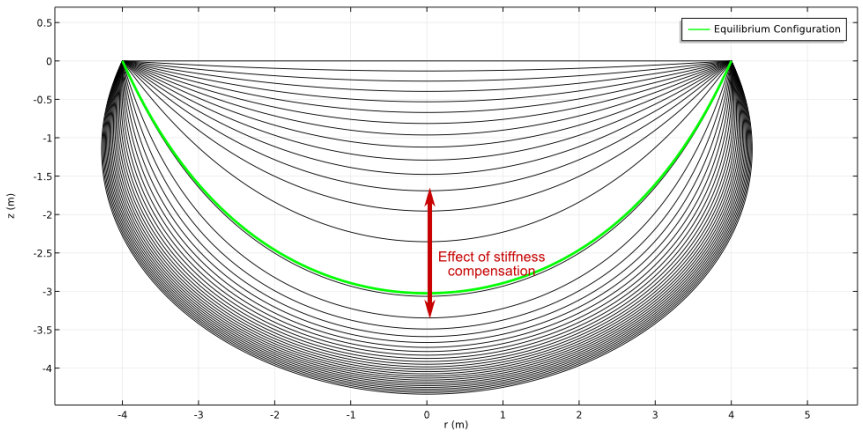

FIGURE 3-5 RESULTS FROM STATIC FEM SIMULATIONS ON THE REFERENCE ICD-DEG, WITH CONSTANT INCREMENTS OF THE OVERLYING WATER HEAD, h_C. THE STATIC EQUILIBRIUM CONFIGURATIONS IS MARKED IN GREEN.

3.3.4.2 EFFECT OF CURRENT AND POWER OUTPUT CONSTRAINTS ON THE DEVICE PERFORMANCE

In the following, we investigate the effect of limiting the maximum current and power output of the DEG (with respect to pursuing instantaneous DEG charging/discharging) on the system dynamics and performance.

We make reference to a regular sea state featuring wave period T=6.5 s and height H=3.5 m. The assumed control strategy is that described in previous sections.

Basing on the considerations outline in previous sections, and assuming a maximum admissible output voltage V_{max}=100 kV the number of layers is set to n_L=130.

First, the optimal value of the electrical partialization, β, is optimized, making reference to the case with no restrictions on the maximum output current/power. The optimal value of the partialization results in β=0.76 and the resulting unconstrained WEC power is 125.3 kW.
Successively, a simulation is run, using the same sea state and the previously optimized value of β, including the following constraints on the maximum power and current: I_{max}=1.6 A, P_{max}=2 MW. The resulting power is 114.2kW, i.e., 8.9% lower than the unconstrained one. This result demonstrates that the considered constraints provoke a reduction in the produced power, therefore, the device conditioning electronics should be properly sized compromising between technological requirements (e.g., limiting the ratio between the maximum instantaneous power and the mean expected peak power handled by the electronics) and energetic performance.
With reference to a single wave period, the ICD-DEG voltage profile in the unconstrained case and in the constrained case is shown in Figure 3-6.
The plot shows that, while rising and falling to zero instantly in the unconstrained case, the voltage rises and falls progressively when constraints are considered. The same effect can be seen making reference to a charge-voltage Q-V plane.
Figure 3-7, in particular, shows the operating ICD-DEG constraints on the Q-V plane and the steady-state periodic trajectories corresponding to the two described simulations. In the unconstrained case, being charging/discharging instantaneous, such operations take place at constant ICD-DEG capacitance, and they are represented by straight segments on the Q-V plane. In the constrained case, on the contrary, charging/discharging take place in a finite time, during which the ICD-DEG moves, therefore such operations are represented by non-trivial curves on the Q-V plane.

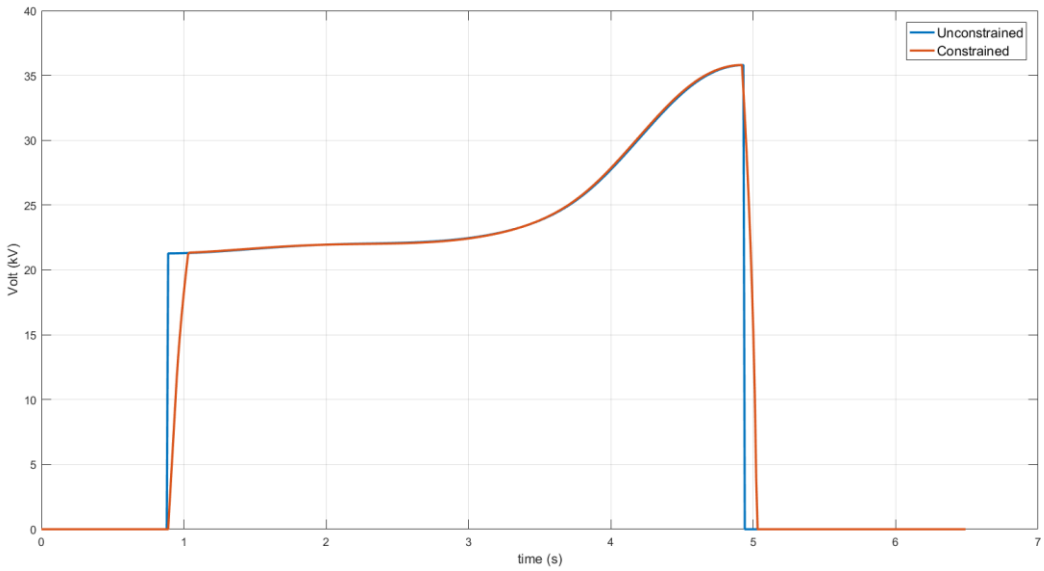

FIGURE 3-6 ICD-DEG VOLTAGE PROFILE (UNCONSTRAINED AND CONSTRAINED CASE)

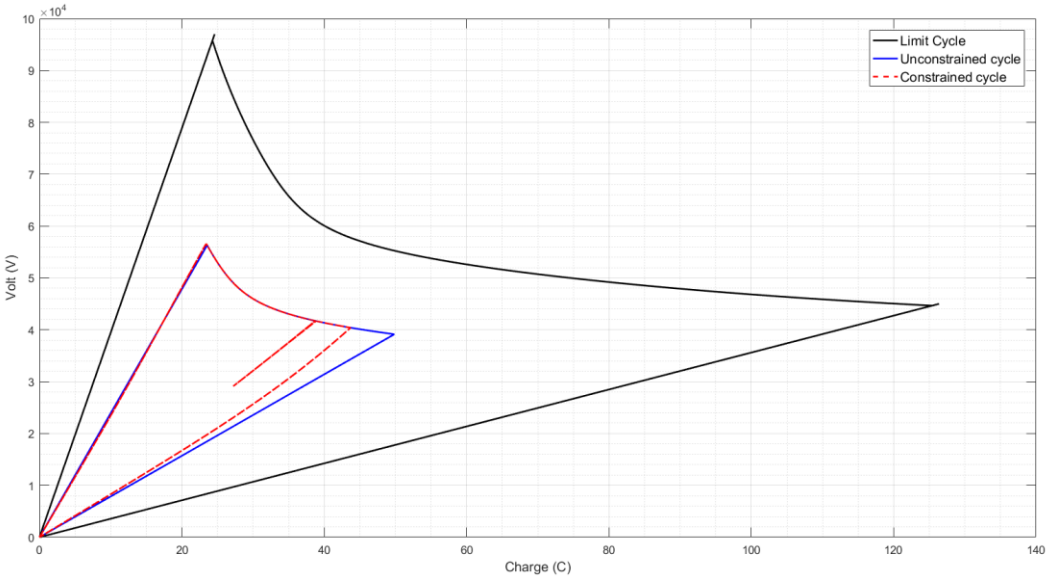

FIGURE 3-7 CONSTRAINED AND UNCONSTRAINED GENERATION CYCLE ON Q-V PLANE .

3.3.4.3 POWER MATRIX COMPUTATION

In this section we report the electrical power that a DrumWEC device, whose dimensions are specified in Table 3-1, can produce. Twelve monochromatic sea states are investigated and a simplified control strategy is assumed, as illustrated in Sec. 3.1, i.e. an optimal electric field's partialization coefficient β is found for every sea state.

Figure 3-8 shows the power matrix (power expressed in kW) for the unconstrained case, with the optimal partialization coefficient β reported into parentheses for every sea state.

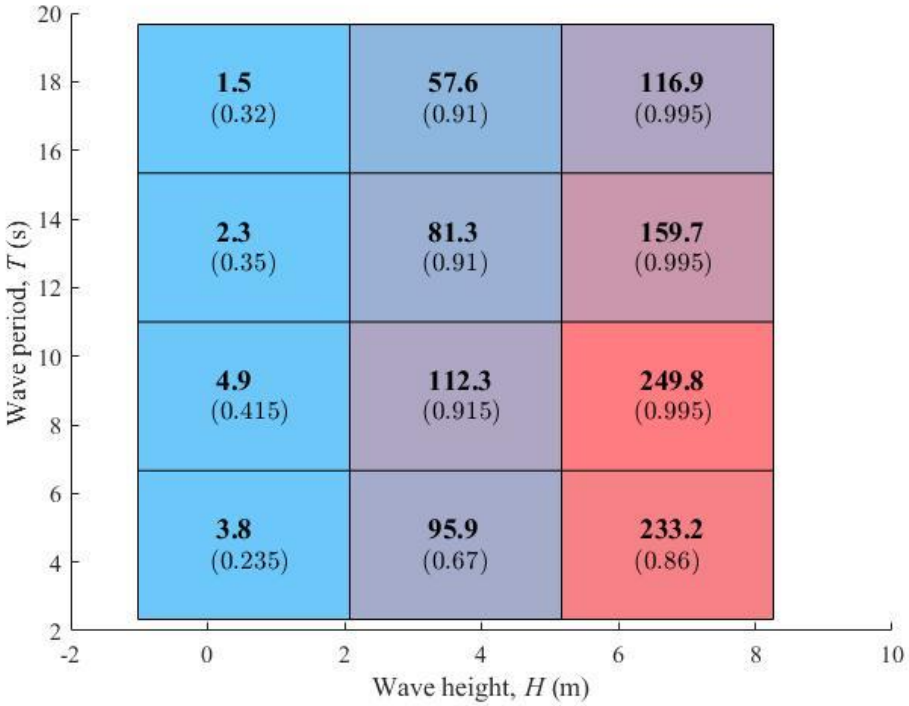

FIGURE 3-8 POWER OUTPUT MATRIX (KW) FOR THE UNCONSTRAINED CASE. THE ELECTRIC FIELD'S PARTIALIZATION COEFFICIENT IS INTO PARENTHESES.

Although the employed control strategy is rougher with respect to the implementation of an optimal control, like real-time MPC, discussed in Sec. 3.2, an improvement of the power output with respect the case in which the electric field's partialization coefficient is kept constant throughout the sea states can be seen. If we hold β=0.69 for every sea state, for example, it can be seen from Figure 3-9 that the power output is always lower than that in the optimized case (Figure 3-8).

Figure 3-10 shows the power output matrix taking into account the constraints on the maximum power and current: I_{max}=1.6 A, P_{max}=2 MW. From the comparison of the two power matrices (Figure 3-8 and Figure 3-10) it is evident that the limit on the maximum module of current and power applied on the DEG reduces the maximum power output achievable by the device.

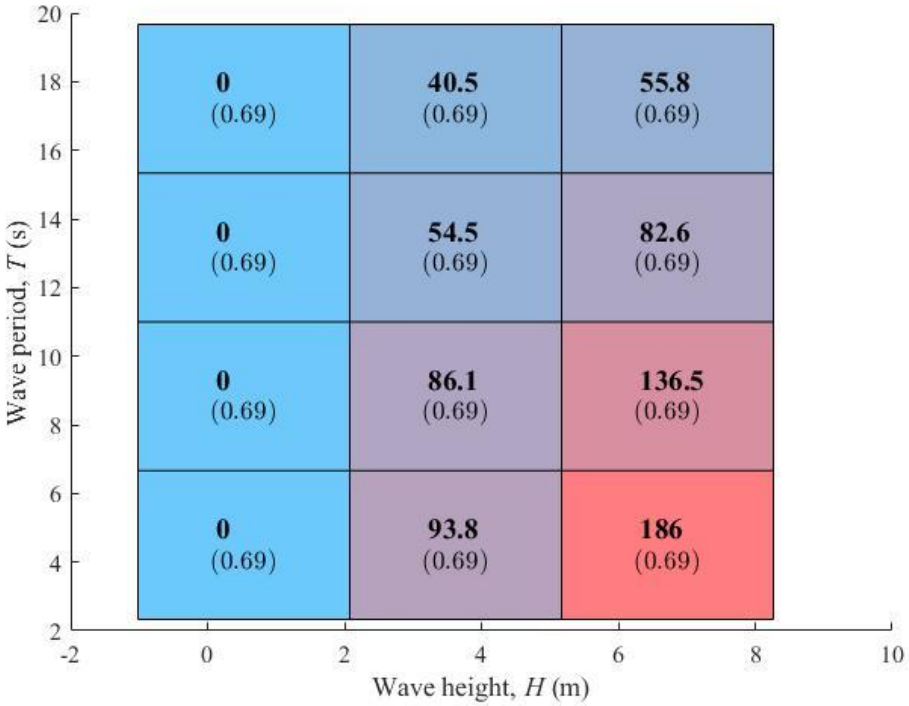

FIGURE 3-9. POWER OUTPUT MATRIX (KW) FOR UNCONSTRAINED CASE, WITH HOLD ELECTRIC FIELD'S PARTIALIZATION COEFFICIENT.

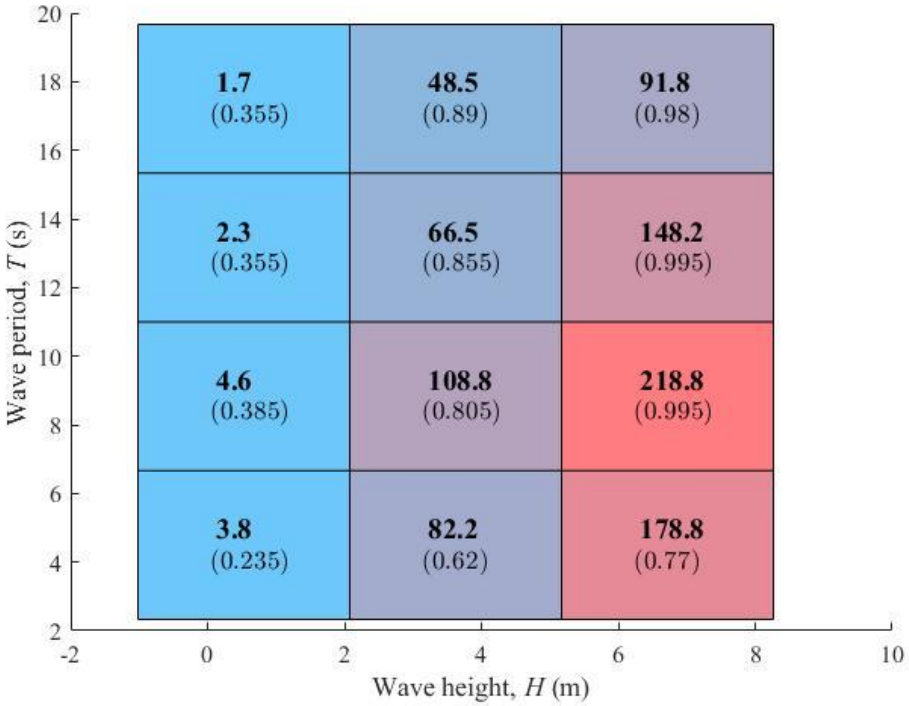

FIGURE 3-10. POWER OUTPUT MATRIX (KW) FOR CONSTRAINED CASE. IN PARENTHESIS THE ELECTRIC FIELD'S PARTIALIZATION COEFFICIENT.

4. Development of HIL setup: preliminary work

4.1. Introduction

This section reports on a detailed description of the HIL system and the current status of activities for its development. The focus here is set on the concept, the technology development, and the experimental short-term laboratory testing of a small-scale physical model to validate and optimize system form, functionality, behaviour and performance. Results of these activities are going to be used to identify and correct unforeseen design and performance issues at an early stage, build confidence and inform the next scale of testing.

Specifically, the aim is to develop a fully functional DEG-PTO system that includes: Energy Conversion Unit (ECU), power electronics, and controller with required sensors. Aiming at full-scale single systems with power output in the range of 100kW to 400kW, the scaled DEG-PTO that will be developed and experimentally investigated in this WP will have a scale in the range of 1:15 to 1:25 and a power output in the range of 1.5W to 10W. The complete scaled DEG-PTO is going to be mounted in a purposely developed HIL set-up that enables it to be tested, with its controllers, in combination with emulated OWC and PD WECs subjected to realistic sea wave conditions. Major objectives of these tests are: 1) the characterization of the static and dynamic response of the DEG-PTO; 2) the assessment of system maximal control force capability and energy conversion efficiency across the entire load regime; 3) the demonstration of system survivability in extreme wave conditions.

The HIL scheme that is needed for such kind of tests set-up has been purposely designed and is going to be built in the next months. The setup comprises:

- a DEG-PTO, sensors to measure current, voltage, and other relevant variables for DEG-PTO evaluation (for instance, pressure sensors, voltage probes and a high-speed camera to keep track of the deformation of the ECU);
- a custom hardware, made of an upper cylindrical chamber open to ambient air pressure and a lower closed cylindrical air chamber with variable geometry regulated by means of an actuated piston (for instance using an electro-cylinder);
- HIL set-up control software and power electronics that implements real-time hydrodynamics models of specific WEC architectures and command the activation status of the ECU simulating the controller of the system.

A commercial real-time target computer with I/O modules (such as a Speedgoat performance real-time target machine) will be used as the control hardware for both the HIL set-up and the DEG-PTO. A similar architecture has been already validated in preliminary experiments in [17].

In the following we report the developments on the following main aspects of the HIL setup:

a. Mechanical system

b. Power/control electronics

c. DEG-PTO

4.2. Mechanical system

The reference ECU is as the inflatable circular diaphragm as described in Section 2.1 that undergoes out of plane expansion when its opposing sides are subjected to a pressure difference.

The design and optimization of the complete and fully functional setup for the small-scale DEG-PTO has been initiated from the preliminary dimensioning of the system. The aim is to obtain appropriate system dimensioning with a rational scaling of its dynamic response.

Our design strategy started from the definition of a nominal power generation requirement of the DEG. A target nominal power of WN=5 W was chosen that is a representative of a scaling between 1:15 and 1:20 of a 100-200kW real device.

The maximum working voltage for real scale devices is foreseen to be in the range of 10-30kV. For this scaled prototype 10kV has been chosen as a trade-off. Such a value is enough to effectively represent the real scale issues of electronics and components, but at the same time it does not set very strict requirements for the safety of the laboratory setup.

Once the target power and the working voltage are decided, it is possible to define the target capacitance of the ECU. In particular, considering that the capacitance is changing roughly by five times from the initial value (flat membrane) when the membrane is fully inflated, a choice of a minimum capacitance Cdm= 100nF and a maximum CdM= 500nF lead to the required energy converted per cycle.

The same capacitance variation can be obtained with different combinations of thickness and radius of the dielectric layers. From the electrical point of view the choice is rather free, on the contrary from the point of view of the dynamic response this choice can have great effect on the corresponding real scale device. The problem has been previously studied and the result bring to optimal combination of thickness/radius that are quite different with (1) the type of WEC device; (2) the employed DE materials, (3) the pre-stretch of the membrane. In any case, the following dimensions of the membrane allow to implement a sufficiently accurate (small-scale) representation of most of the combination of materials and devices:

(1) Diameter: 0.35-0.45 m
(2) Thickness: 0.2-1.0 mm (two to four layers of dielectrics)

The target mechanical system has to be able to induce appropriate mechanical loading on the membrane in order to induce a variation in the capacitance of the DEG as illustrated in the previous section. The volume displacement per cycle is given by simple geometrical relations that take into account the variation of volume of the (quasi) spherical cap in the inflated condition.

Specifically,

$$V = 2V_s = \frac{4}{3}\pi r^3 \tag{4.30}$$

Where V is the required volume displacement per cycle, V_s is the volume of the hemispherical cap when fully inflated, and r is the radius of the DEG membrane.

The required pressure loads required to fully deform the ECU membrane is calculated by appropriately scaling of previous experimental results obtained on a smaller scale setup (with a membrane diameter of 0.13 m).

In the case of a 0.13 m membrane with a thickness of 0.2mm, the maximum pressure required for reaching a fully deformed configuration - target deformation is achieved when the displacement of tip of the membrane is equal to the radius - was roughly 5 kPa.

In the setup that is designed in this project, the target membrane radius is in the range of 0.15- 0.25 m so results obtained for the 0.13 membrane have to be scaled. If the geometry of the membrane is scaled up geometrically, i.e. thickness is increased of the same proportion of the radius, the pressure that is needed for the deformation remains constant and the power of the device assumes the values represented in Figure 4-1.

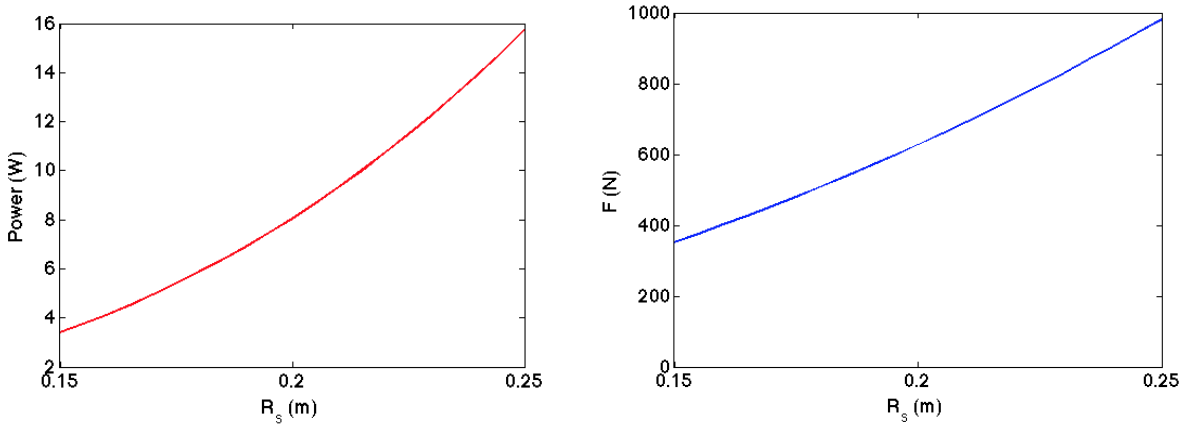

FIGURE 4-1: ESTIMATED POWER VS RADIUS OF THE MEMBRANE (LINEAR GEOMETRICAL SCALING) OUTPUT AND FORCE REQUIRED AT THE LINEAR STAGE OUTPUT IN ORDER TO OBTAIN THE FULL DEFORMATION OF THE ECU MEMBRANE.

In order to implement such required performances, the rational choice brings to consider a system that implements the linear displacement of the piston through the combination of a rotational motor and a linear stage.

The choice of appropriate combination of motor/driver and linear guide has been conducted with a certain level of safety margin which takes into account possible detrimental contributes of friction of the piston seals.

The components that were chosen are the following:

- Motor: Low Inertia Brushless, Kollmorgen AKM52L, power of 2.3kW, nominal speed of 3500 rpm;
- Driver: Kollmorgen AKD-P01206, power of 4kW, EtherCAT communication, with on board position controller;
- Linear stage: Festo, ball-guide with a maximum linear force of 4500N and maximum speed of 1.2m/s.

The chosen performances of these components make it possible to meet the requirements of force, speed and power with very large safety factor. This choice is done to introduce flexibility in the design options for the ECU membrane and in view of the possible implementation of larger scale/power systems.

The design of the mechanical assembly is represented in Figure 4-2. The motor has been placed on the top of the setup in axis with the linear stage. The output of the linear stage is connected to a piston that

moves in an air cylinder inducing the air to flow forward and backward in a duct. The duct is U-shaped in order to guarantee easy access to the output flange were the DEG is attached. The DEG is mounted on a plexiglass cylinder.

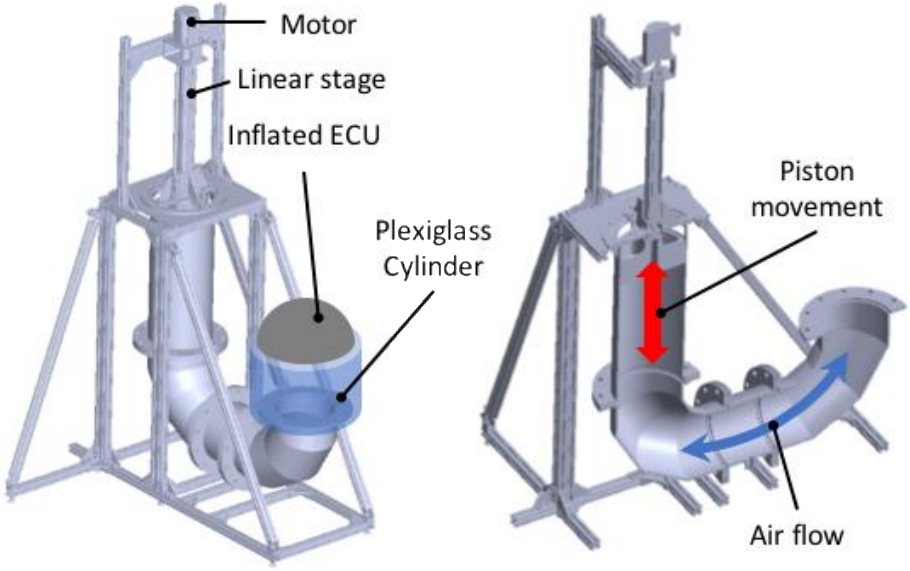

FIGURE 4-2: FINAL LAYOUT OF THE HARDWARE-IN-THE-LOOP WITH VERTICAL PISTON

Currently, the main components of the equipment such as motor, driver, linear stage and sensors have been acquired and the custom mechanical components are manufactured.

A preliminary picture of the piston assembly is presented in Figure 4-3.

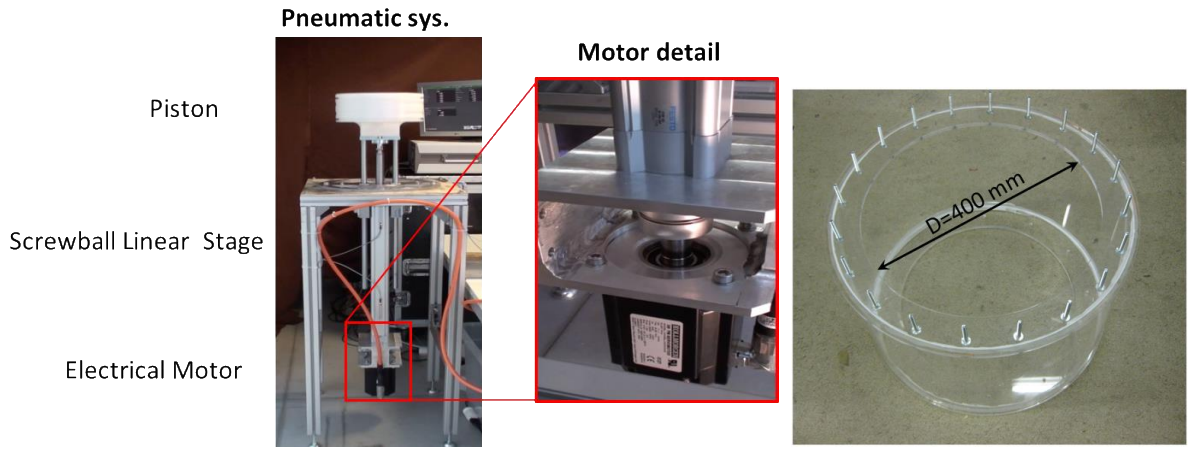

FIGURE 4-3: ASSEMBLY OF THE PNEUMATIC ACTUATION SYSTEM AND DETAIL OF THE ELECTRICAL MOTOR CONNECTED TO THE LINEAR STAGE (LEFT); PICTURE OF THE ELECTRONICS PROTOTYPE DURING TESTING.

4.3. Sensing, control and power electronics

A MatLab xPC Target real-time machine is employed as main controller of the system. Specifically, a Performance real-time target machine by SpeedGoat. is employed to run real-time routine. The device shows the following characteristics:

- Performance real-time target Intel Core 2 Duo 2.13GHz CPU, 2048MB RAM, 1024MB industrial grade SATA Flash device;
- 8 differential analog output channels, fast 16-bit analog module with (module IO108-Performance);
- 16 differential simultaneous sampling analog input channels with high-resolution 18-bit successive approximation (SAR), supporting up to 1000 KSPS per channel (module IO112-16-Performance)
- 6 x PWM generation and 8 x QAD (Quadrature Decoding) plus 1 x Interrupt and 1 x Negation (IO311-PMW6TTL/NEG1TTL/INT1TTL module).

The main functionalities of the real-time control system can be summarized as follows:

(1) run the real-time hydrodynamic model of the plant, which governs the motion of the piston, and to control the charging status of the CD-DEG;
(2) command the position of the piston that is used to induce the deformation of the ECU membrane to the motor driver (model AKD-P01206 of Kollomorgen);
(3) control the power-electronic in order to timely command the charging and discharging of the ECU;
(4) acquire the relevant data that are required to post process the experiments
(5) provide to an external scientific camera with a trigger signal to synchronize the data acquisition with the videos.

Real-time software is generated through Matlab-Simulink and loaded on the target machine. The use of Simulink gives more flexibility and allows to perform many different kind of test easily reducing the development time of different experimental procedures. After test execution, the data collected from the real time target are transferred to the PC via Ethernet communication.

Preliminary tests have been conducted in order to verify the real-time performances running a sample hydrodynamic model of a 2 DoF floating oscillating water column. The sample model simulation was set to acquire (while running the hydrodynamic model):

- 8 analog differential input signals at 16-bits (only 4 of them are strictly needed for pressure and voltage measures) and take derivatives of all of them;
- drive 4 PWM output at 100kHz (only two are strictly required to drive the two low voltage and high-voltage stages of the power electronics);
- drive 4 I/O ports at sample frequency (only one is strictly required to trigger the Camera);
- 1 opened EtherCAT (bidirectional) communication channel to drive the piston motor;

A minimum refresh rate of 2 ms (corresponding to 500 Hz of sample frequency) has been obtained, which is a value that is considered (more than) satisfactory for the representation of the dynamics of the system. However, such sample time could be further improved by customizing the EtherCAT protocol or driving the motor through analog signals.

The sensing system is composed by the following sensors:

- Voltage probes: In order to sense the voltage on the DEG and on the primary stage of the power electronics two custom made HV probe have been implemented that features very high input resistance (nearly 50GOhm), which drastically limits the drain of charge from the DEG electrodes, and large bandwidth, which is obtained thanks to a capacitor compensation network. In order to minimize the current leakage of the power electronics, all the HV wirings and

components have been encapsulated via thick layers of silicone gel (Magic gel by Raytech) and acrylic tape (VHB 4905 by 3M.).

- Pressure sensors: The chamber is equipped with pressure sensors that are employed (1) to collect pressure data during the operation of the device for validation purposes and (2) to implement controllers that decide the activation status of the ECU on the base of the pressure and its derivatives.
- Camera: In order to track the deformation of the ECU membrane a scientific camera is employed the camera is going to be located at position and orientation with respect to the ECU membrane and thanks to image post-processing analysis that have been previously developed the displacement of the tip of the membrane is going to be acquired. This is going to be used to validate models and to implement controllers that make use of the tip displacement to decide the activation status of the ECU. A camera ECU Point Grey GS3-U3-23S6M-C with lens 250F6C, using acquisition software FlyCapture 2.9 is going to be employed.

4.4. DEG-PTO fabrication study and tests

4.4.1. Fabrication test of silicone solid-state ECU

This sub-section illustrates a fabrication process of DEGs that has been conceived and studied in order to produce a functional and reliable DEG-PTO to be employed in the test campaign.

The device is based on the dielectric elastomer produced by the multinational company Wacker Gmb. [18]. This dielectric film has been chosen for the following reasons:

(1) This is the first commercial product that has been purposely developed for the application of DEGs;
(2) It is a silicone-based product that makes it possible to integrate silicone made conductive electrodes;
(3) The material's performances (form datasheet) are very promising in terms of dielectric constant and electrical break-down limit.

We should however underline that the current cost of this material (more than 100€/kg) is too high to be eligible for an effective economic deployment. Nevertheless, we have also to consider that the current production costs are those of a prototype material for niche laboratory applications, and a large room for improvement could be determined by future economy of scales.

Wacker film is available in rolls of 250mm in width. Among the available thickness we chose to obtain the dielectric layer of the DEG with two films of 100μm for a total un-stretched thickness of 200μm. The electrodes are prepared and deposited through a procedure that is described in the following.

This choice of having the dielectric made of two films is done to facilitate the fabrication process of the electrodes. Actually, during the deposition of the electrode the dielectric film is firmly fixed on a flat surface. The electrodes are deposited separately on two different pieces of dielectric and are assembled as they are mounted on a circular frame that is employed to hold the ECU in operational conditions.

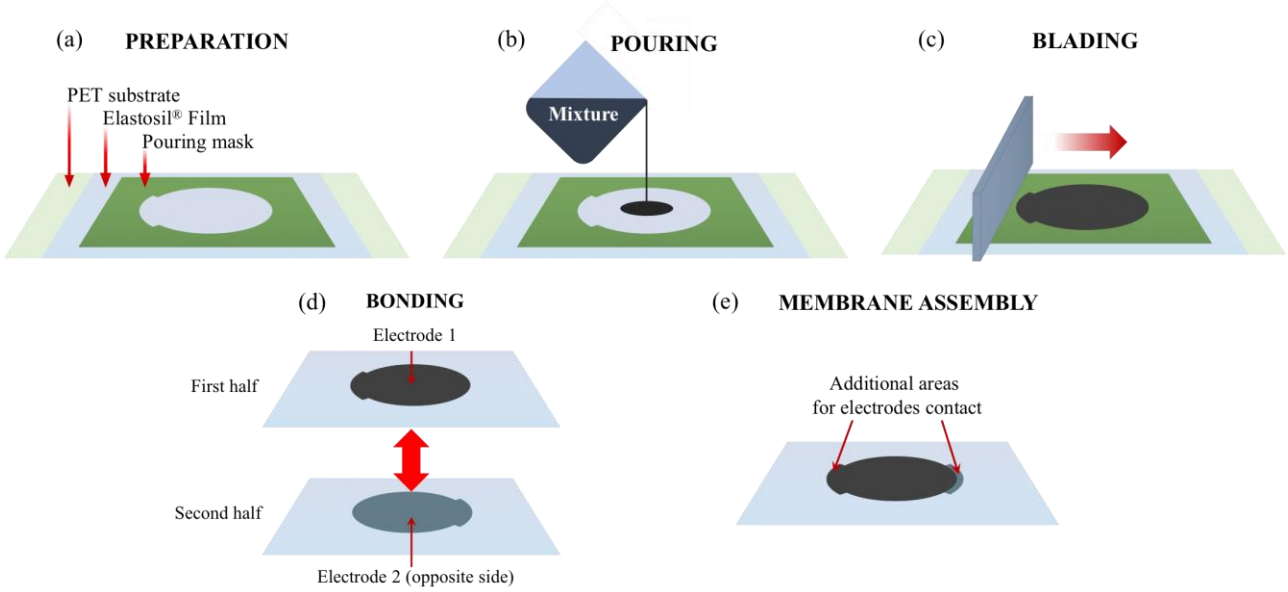

FIGURE 4-4: PHASES OF THE PREPARATION OF THE ELASTOMERIC ELECTRODE: (A) POURING MASK WITH SHAPED CUT IS LAID ON THE ELASTOSIL® FILM (THAT IS KEPT ON ITS PET SUPPORT), (B) MIXTURE OF PDMS, CARBON BLACK AND ISOPROPANOL IS POURED; (C) THE EXCESS OF MATERIAL IS REMOVED BY BLADING

The conductive layers are prepared starting from a dense liquid compound that is poured directly on top of the Elastosil sheet using a plastic mask to obtain the desired electrode shape and thickness.

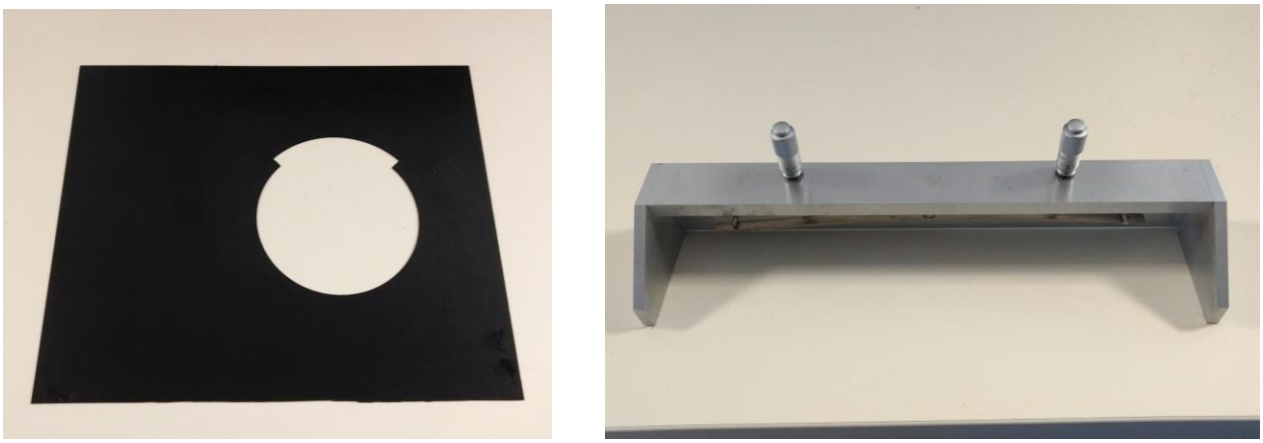

FIGURE 4-5: PICTURES OF THE TOOLS THAT HAS BEEN EMPLOYED FOR THE PREPARATION

The electrode compound is liquid when poured, for this reason the substrate must be fixed on a flat surface which is kept horizontal until the compound is completely polymerized in order to obtain a uniform thickness conductive layer. The polymerization of the compound is accomplished in about 12 hours at ambient temperature. Within this time the electrode loses more than ¾ of the original thickness. To obtain an electrode 80 − 100μm thick the original thickness of the mask is 400μm. At the end of polymerization the conductive layer is perfectly bonded to the dielectric substrate, provided that it has been perfectly cleaned with iso-propilic alcohol (IPA). After pouring the compound into the mask, a blade is used to remove the excess of material in order to obtain a uniformly thick electrode. This process is made in parallel on two substrates. After the polymerization is complete, the two substrates are bonded together just putting them one on top of the other. The two surfaces must be perfectly clean and the contact with hands must be avoided.

The electrode compound is made from silicon with carbon black particles dispersed. This is the fabrication process:

1. Put the planetary shaker container on a scale.
2. Put 0.8g of carbon black powder 8g IPA and 6 stainless steel sphere with 12mm diameter.
3. Close the container into the shaker and run the shaker for 10 minutes. This allow to grind the carbon black and make very small carbon black particle well dispersed into the solvent.
4. When finished put 8g silicone Wacker Silgel RT 625 (7.2g A+ 0.8g B), put 8g IPA into the container.
5. Close the container into the shaker and run the shaker for 10 minutes.
6. Pour the compound into the mask. Don't wait too much because the solvent which is very volatile will evaporate changing quickly the viscosity.
7. Pass the blade on to the mask to remove the excess of compound.
8. Wait 12 h.
9. Bond the two substrates together.

If a different quantity of compound is required, just keep the same proportion of reagents. In order to achieve a successful fabrication process, this must be kept in a clean place.

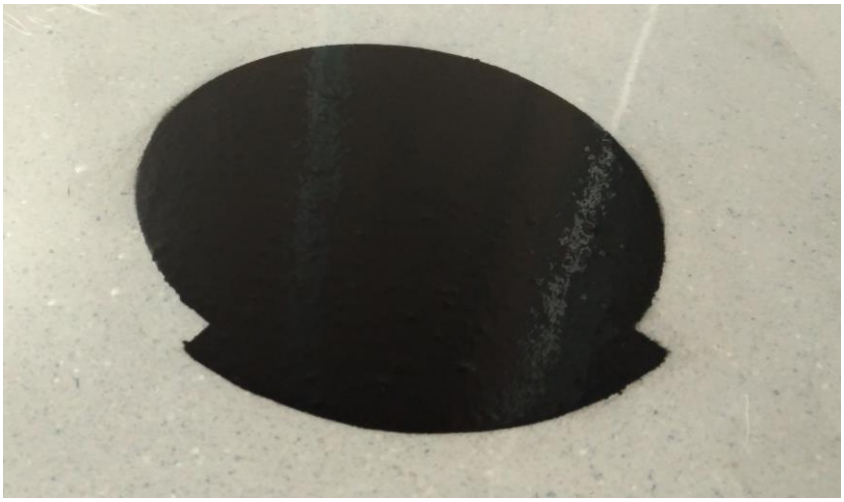

FIGURE 4-6: PICTURE OF THE OBTAINED ELECTRODE

4.4.2. Performance evaluation

The membrane assembly (see Figure 4-7) is mounted on an holder made of two annular rings (with internal diameter of 130 mm) that are bolted in a way to squeeze the external boundary of the DEG membrane. A flanged tube is then inserted and screwed in the ring-holder in way to produce an out-of-plane deformation of the membrane and inducing equibiaxial stretch in its central area of $\lambda_p = 1.15$. The diameter of the electrodes is such that when the assembly is completed it equals the internal diameter of the flanged-tube employed for pre-stretching. Eventually, a further ring-shaped holder is bolted on the top in order to avoid slipping at the border of the membrane. The contact with electrodes is ensured by copper tape strips that are attached on the top of the flanged-tubes (HV electrode) and on the external ring-shaped holder.

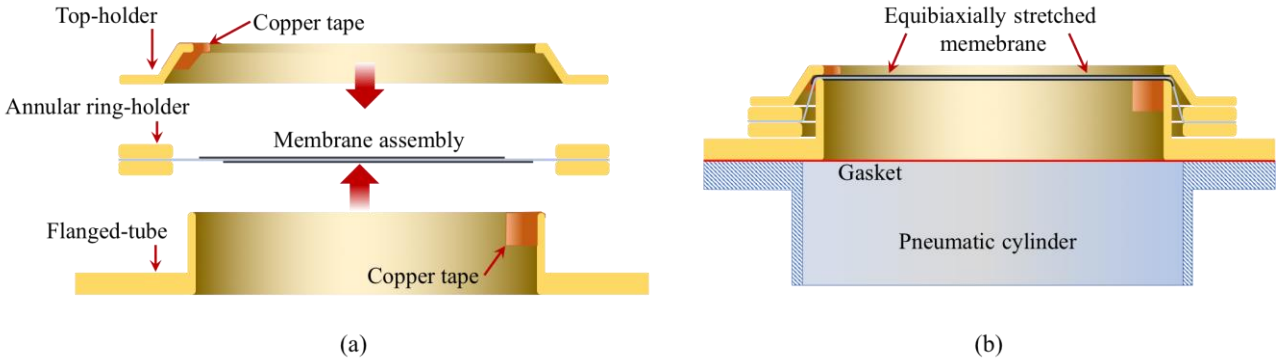

FIGURE 4-7: PICTURE : PHASES OF THE ASSEMBLY OF THE DIELECTRIC ELASTOMER GENERATOR (SCREWS ARE NOT REPRESENTED): (A) MEMBRANE ASSEMBLY IS XED ON ANNULAR RING HOLDER; (B) FLANGED-TUBE AND TOP-HOLDER ARE INTRO-DUCED AND THE ASSEMBLY IS XED ON THE OUTPUT FLANGE OF THE PNEUMATIC CYLINDER.

A DEG assembly, prepared with described procedure, is fixed on a test-bench that has been designed for the testing and characterization of ICD-DEGs [24] (see Figure 4-8). The test-bench comprises a mechanical sub-system that make it possible to in inflate and deflate the DEG membrane; a high-voltage (HV) electronics combined with a real-time controller that make it possible to drive and synchronously acquire sensor readings. The main component of the mechanical sub-system is a pneumatic system made of an air tight and a movable piston with a diameter D=130 mm, that slides into a polycarbonate cylinder tube (with internal diameter D = 130mm) with a flange on the top that makes it possible to fix the DEG assembly. Air leaks are minimized by using a planar annular gasket and a tight screwed fixing on the DEG assembly side and appropriate pneumatic circular seals on the piston side.

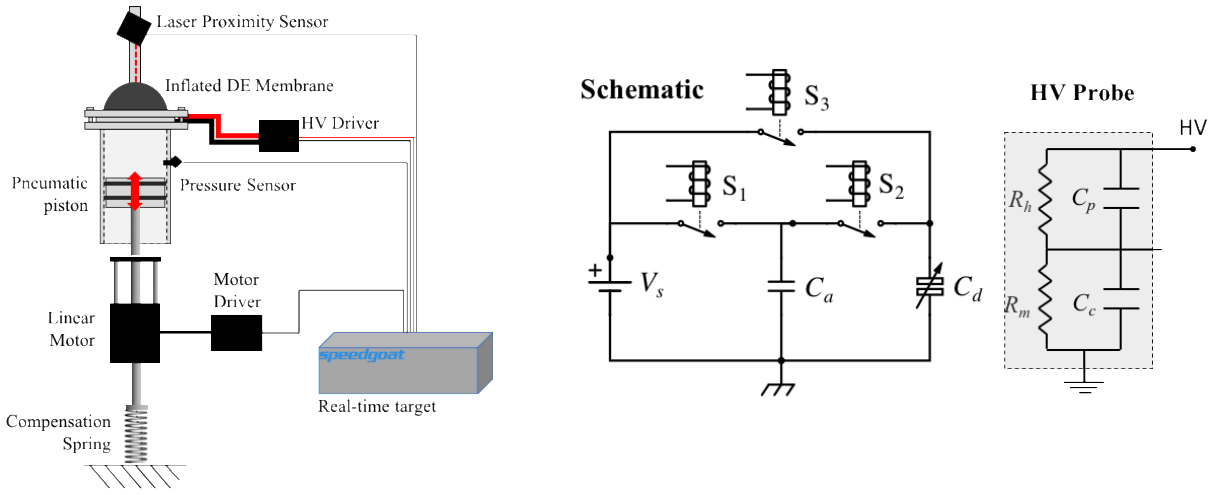

FIGURE 4-8: SCHEME OF THE SETUP EMPLOYED FOR THE PRELIMINARY CHARCTERIZATION AND TESTING OF THE FABRICATED MEMBRANE.

The pneumatic system is actuated via a brushless linear motor (P01-37x120F/200x280-HP by LinMot), with embedded encoder that is used to measure piston position, x. A pressure sensor (MPX12 by Freescale Semiconductor) installed on the cylinder tube is used to measures the differential pressure, p, between cylinder chamber and ambient air. A high-speed high-accuracy CCD laser displacement sensor (LK-G152 by Keyence), which is mounted on top of the cylinder head, is employed to measure the DEG tip displacement, h.

The pneumatic cylinder is mounted vertically and an elastic spring is introduced in order to compensate for the weight of both piston and motor slider. The electrical control of the DEG is implemented through an HV power and sensing electronics whose topology is represented in Figure XX. The considered driving electronics comprises a four-quadrant high-speed HV power amplifier (Trek 10/10B-HS) and an HV reed relays box (equipped with three HM12-1A69-150 by MEDER electronic) that alternatively connect the DEG electrodes to either the power supply or to the additional capacitor. In the circuit, resistor are also used to limit the peak current that occurs during charges and discharges but these are not represented in the schematic.

To measure the electric potential difference, V_d, between DEG electrodes, a custom made HV probe has been implemented that features very high input resistance (nearly 50GΩ), which drastically limits the drain of charge from the CD-DEG electrodes, and large bandwidth, which is obtained thanks to a capacitor compensation network (see the high voltage probe schematic reported in Figure 4). In order to minimize the current leakage of the power electronics, all the HV wirings and components have been encapsulated via thick layers of silicone gel (Magic-gel by Raytech) and acrylic tape (VHB 4905 by 3M).

A real-time machine (Performance real-time target machine by SpeedGoat) running the MatLab xPC Target software environment is employed to control both the motion of the piston and the charging status of the DEG, i.e. HV power supply and relays). This set-up enables to command any complex prole for piston position, z, and DEG voltage, V_d , which can be generated via software on the basis of available measurements and properly defined models. For DEG characterization purposes, in this work, the position of the piston is simply controlled according to trajectories with constant velocity prole with different amplitudes in displacement, z_p. The DEG voltage is controlled according to energy harvesting cycles. Specifically, the generation cycle is implemented as following this sequence of operations. The switches S_1 and S_2 are opened, S_3 is closed and the voltage of the supply is set to V_s = 0, i.e. the DEG voltage is also V_d = 0. The piston is moved upward of a quantity z_p consequently the DEG membrane is inflated, i.e. the capacitance is increased to a value C_h. The switch S_3 is opened, i.e. the DEG is isolated and S_1 is closed and the capacitor C_a is charged, with a voltage supply V_s=V_0 during this operation the piston keeps its position). The capacitor C_a is disconnected from the power supply by opening S_1 and connected to the DEG by closing S_2, thus the DEG is rapidly charged up to a voltage V_2. Then the piston returns to its home position and the DEG (in parallel with C_a) increases its voltage to V_3 and reaches the flat configuration, corresponding to the state where DEG exhibit minimal capacitance C_l. Lastly, the DEG is isolated by opening S_2 the supply voltage is set to V_s = 0 and the DEG is discharged by closing S_3 draining charge through the (bidirectional) power supply.

Experiments have been conducted for increasing value of supply voltage V_0 and of piston displacements z_p respectively in the ranges of 1-9 kV (with increment of 0.5 kV) and 0-80 mm (with variable increments).

Generation cycles are represented in Figure 4-9 where Q-V cycles are reported for different levels of inflation.

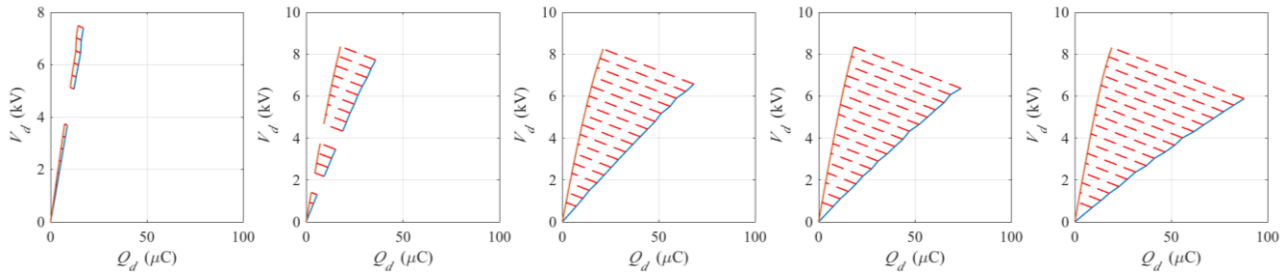

FIGURE 4-9: GENERATION CYCLE REPRESENTED ON THE COMPLEX CONJUGATE PLANE (Q-V PLANE)

The following figures of merit have been calculated and derived from the measurements.

- Electrical energy that is converted in each generation cycle

$$E_{j,k} = \oint V_{d_{j,k}}\, dQ_{d_{j,k}} \approx \frac{1}{2} C_a \left(V_{3_{j,k}}^2 - V_{2_{j,k}}^2\right) + \frac{1}{2} C_l V_{3_{j,k}}^2 - \sum_{i=1}^{k} \left(C_{h_{j,i}} V_{2_{j,i}} - C_{h_{j,i-1}} V_{2_{j,i-1}}\right) \frac{V_{2_{j,i}}^2 + V_{2_{j,i-1}}^2}{2} \quad (4.31)$$

  where the subscript j indicates the j-th level of inflation and k indicates the k-th applied voltage level. Formally, voltage $V_{2_{j,k}}$ in equation (4.31) should be considered equal to 0 at k=0.

  Note that this estimation takes into account the so-called actuation-like behavior when the priming is performed.

- Density of energy is defined as $e = E_{j,k}/m_d$, *with* m_d being the mass of active dielectric material that is employed.
- Conversion factor $\eta = E_{j,k}/W_{j,k}$ where $W_{j,k}$ is the mechanical input work that is done by the pneumatic piston.

$$W_{j,k} = \oint p_{j,k} A_p dz_{j,k} = \pi r_p^2 \oint p_{j,k}\, dz_{j,k}$$

The results of experimental tests are reported in Figure 4-10, where energy converted per cycle, energy density and conversion factor for different level of inflation are reported against the supply voltage, i.e. initial voltage of the additional capacitance before priming.

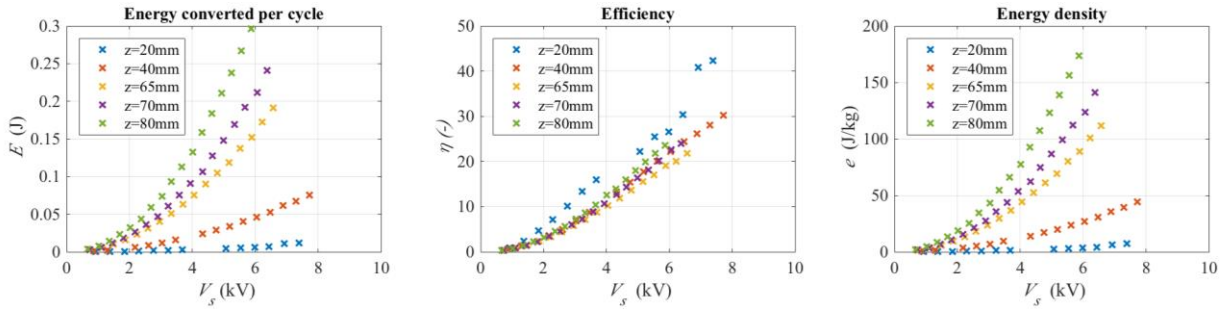

FIGURE 4-10: FIGURES OF MERIT FOR DIFFERENT INFLATION LEVELS CALCULATED AS AVERAGE ON FOUR CYCLES ARE PLOTTED AGAINST SUPPLY VOLTAGE: (A) CONVERTED ENERGY ; (B) ENERGY DENSITY ;(C) CONVERSION FACTOR.

Values as ahigh as 0.3 J for the converted energy per cycle and 160 J/kg for the energy density are achieved. Both the figures of merit are monotonically increasing with the voltage. Specifically, typical quadratic-shaped response can be observed for the energy and energy density. As expected, converted energy increases with the level on inflation of the DEG membrane.

As for the conversion factors, one can notice that values as high as 52 % are reached in the case of smaller inflation levels and they reache 20-30% for larger inflation levels.

Such efficiency values are already quite promising, but a further discussion should be introduced since a in depth observation on the estimantion preocedure could highlight more positive expectations.

First, the contribution of electrical to efficiency reduction shoould be negligible since charge loss are as small as 2-3% (see Figure 4-11). This corresponds in terms of energy of a loss in worst conditions of 7-9%.

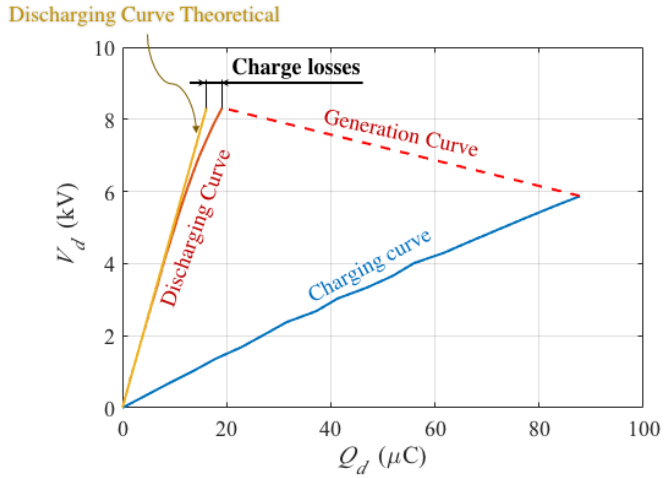

FIGURE 4-11: Q-V PLOT FOR THE CYCLES WITH HIGHEST ELECTRIC FIELD IMPOSED THAT GENERATES THE MAXIUM ELECTRICAL LOSSES.

Thus, the greatest share of energy losses are attributable to mechanical aspectes aspects. Two contributes are here involved. Hysteresis losses in the material that are real losses which are affecting the perfromances of the system. Second, air leakages due to imperfecft tightness of piston sealings are actually accounted as efficiency losses but should not be considered as real losses since in real system they are going to be negligible sincde pressure is going to be lower.

Throug an coarse characterizatin of air-leakages done through the observation of presssure during the generation cycles, we can undertand that most of the losses can be atributed to this phenomena. Thus, real efficiency values at larger scale are expected to be much more promising than the one presented in Figure 4-10.

5. Conclusions

5.1. Conclusions

In this document, we present the work conducted in the framework of the WP 5 of the Project. The activities are here focussed on the development of a set of strategic issues for the advancement of the technology of Dielectric Elastomer Generators (DEGs) for Wave Energy Converters (WECs).
Specifically, the activities of this WP concern: (1) the study and development of a power electronics and the associated sensing/control system for a DEG-PTO for WECs; (2) the study of effective controllers for DEG-PTO and (3) the design and development of a laboratory test-bench, employing the developed electronics and control algorithms, that is conceived to perform Hardware In the Loop (HIL) simulations.

Different topologies for the power electronics are analysed considering the most performing DC-DC converters architectures. The chosen solution is a Dual Bridge Bidirectional DC-DC converter based on a multilevel architecture. This takes into account the given design specifications and availability/costs of components. The design of electronic circuit for DEG management is completed. The choice of components and the definition of the control strategies is understood. A further step into implementation has been made. A prototype of one stage of the circuit was built and preliminary adjustments have been performed. The transformer is ready to be mounted. The inductance of the transformer has been measured respecting the expected theoretical values. The future work will be to build and debug the complete DAB circuit in order to define the exact module design and realize multiple copies of DAB modules. As for the sensing solutions a capacitive based method has been assumed. The strategy is based on the superposition of a small amplitude oscillating excitation input on the same DEG and a filtering strategy to accurately evaluate the capacitance.

Additionally, a synthesis approach has been formulated in order to design the generic controller of a DEG-PTO. The proposed approach considers the fully-coupled WEC-DEG interaction dynamic problem and a model that represents the power electronics (with its limitations) that has been presented in this document. A synthetic description of the techniques used to identify the optimum control aimed at maximizing the WEC power in presence of constraints due to the PTO is presented. Successively, we set our attention on a concept of Pressure Differential (PD) WEC, housing a DEG PTO in direct contact with sea water. We present a wave-to-wire model for the system, comprising modelling of the fluid-structure interaction between sea water and the DEG, and the electrostatic response of the DEG, included the electrical losses due to resistive electrodes and leakage currents (see Deliverable D 5.1). Due to the highly non-linear WEC response (due to both the complex fluid-structure interaction and to the electrical losses), the “optimum control” postulated before is very difficult to be mathematically identified and its real-time implementation is infeasible. We thus propose a simplified but yet effective heuristic control strategy, which includes the possibility to regulate the level of electrical loading.

Such control strategies are going to be tested and validated in the framework of the HIL testing campaign that is going to be developed in the next period.

In the last section of this deliverable, the status of the development of the HIL setup is reported. Specifically, the design of mechanical, electronic and control setup has been finalized and the system is currently being integrated.

For what concerns the DEG-PTO prototype, a fabrication procedure has been tested at a smal scale in order to verify the effectiveness of the process. The fabricated DEG-PTO is based on a commercial material developed by Wacker polymers that has been purposely conceived for dielectric elastomer

generators, and it has been equipped with custom-made polymeric compliant electrodes. The developed prototype has been tested showing promising results in terms of energy density and efficiency. The process for the development of an up-scaled system has been initiated.

5.2. Ongoing and plans

In the next period, the setup is going to be integrated and the test campaign is going to start and be completed by the end of 2017. At least two sets of tests are in program.

A first set of tests of the integrated setup with sub-optimal DEG-PTOs. A first sub-optimal DEG-PTO is going to be fabricated using commercial acrylic VHB dielectric membrane. This solution is simpler since the VHB material has been previously/successfully employed by partners of the consortium to fabricate intermediate scale systems. This first prototype is useful to support the integration and testing of the system but it is expected to provide sub-optimal performances due to: (1) higher level of viscoelasticity of VHB material; (2) higher level of conductivity.

In a second set of test a new DEG-PTO is going to be employed. Such a prototype is going to be an up-scaled version of the DEG-PTO that is presented in Section 4 of this deliverable. A fabrication process has been identified and implemented for a DEG PTO that feature a dimension of 13cm in diameter while the final goal is to develop a system in the range of 40 cm in diameter. This step of upscaling should not represent a major challenge since the fabrication techniques that have been implemented are applicable to the larger scale system. This new system is expected to provide improved performance in terms of efficiency and convertible energy density.

BIBLIOGRAPHY

[1] Alves, M. (2012). Numerical simulation of the dynamics of point absorber wave energy converters using frequency and time domain approaches. PhD Thesis. Universidade Técnica de Lisboa.

[2] Viuff, T. H., Andersen, M. T., Kramer, M., Jakobsen, M. M. (2013). Excitation forces on point absorbers exposed to high order non-linear waves. In 10th Ewtec 2013 European Wave and Tidal Energy Conference Series. Technical Committee of the European Wave and Tidal Energy Conference.

[3] McCormick, M. E. (2010). Ocean engineering mechanics. New York: Cambridge University Press.

[4] Vertechy, R., Rosati, G. P. P., Fontana, M. (2015). Reduced model and application of inflating circular diaphragm dielectric elastomer generators for wave energy harvesting. Journal of Vibration and Acoustics, 137(1), 011004.

[5] Holzapfel, G. A. (2000). Nonlinear solid mechanics (Vol. 24). Chichester: Wiley.

[6] Steinmann, P., Hossain, M., Possart, G. (2012). Hyperelastic models for rubber-like materials: consistent tangent operators and suitability for Treloar's data. Archive of Applied Mechanics, 82(9), 1183-1217.

[7] Moretti, G., Forehand, D., Vertechy, R., Fontana, M., Ingram, D. (2014, June). Modeling of an oscillating wave surge converter with dielectric elastomer power take-off. In ASME 2014 33rd International Conference on Ocean, Offshore and Arctic Engineering. ASME.

[8] Moretti, G., Rosati, G. P. P., Alves, M., Grases, M., Vertechy, R., Fontana, M. (2015, May). Analysis And Design of an Oscillating Water Column Wave Energy Converter with Dielectric Elastomer Power Take-Off. In ASME 2015 34th International Conference on Ocean, Offshore and Arctic Engineering. ASME.

[9] Cretel, J. A., Lightbody, G., Thomas, G. P., Lewis, A. W. (2011). Maximisation of energy capture by a wave-energy point absorber using model predictive control. IFAC Proceedings Volumes, 44(1), 3714-3721.

[10] Hals, J., Falnes, J., Moan, T. (2011). Constrained optimal control of a heaving buoy wave-energy converter. Journal of Offshore Mechanics and Arctic Engineering, 133(1), 011401.

[11] Eidsmoen, H. (1996). Optimum control of a floating wave-energy converter with restricted amplitude. Journal of Offshore Mechanics and Arctic Engineering. Transactions of the ASME, 118(2), 96-101.

[12] Rosati Papini, G. P. (2016). Dynamic Modeling and Control of Dielectric Elastomer Generators for OWC Wave Energy Converter. PhD Thesis. Scuola Superiore Sant'Anna, Pisa.

[13] Camacho, E. F., & Alba, C. B. (2013). Model predictive control. Springer Science & Business Media.

[14] Kaltseis, R., Keplinger, C., Koh, S. J. A., Baumgartner, R., Goh, Y. F., Ng, W. H., ... Bauer, S. (2014). Natural rubber for sustainable high-power electrical energy generation. RSC Advances, 4(53), 27905-27913.

[15] Vertechy, R., Fontana, M. (2015). Electromechanical characterization of a new synthetic rubber membrane for dielectric elastomer transducers. In SPIE Smart Structures and Materials+ Nondestructive Evaluation and Health Monitoring. International Society for Optics and Photonics.

[16] Vertechy, R., Frisoli, A., Bergamasco, M., Carpi, F., Frediani, G., De Rossi, D. (2012). Modeling and experimental validation of buckling dielectric elastomer actuators. Smart Materials and Structures, 21(9).

[17] Moretti, G., Rosati, G. P., Fontana, M., Vertechy, R. (2015, May). Hardware in the loop simulation of a dielectric elastomer generator for oscillating water column wave energy converters. In *OCEANS 2015-Genova* (pp. 1-7). IEEE.

[18] Ultrathin Silicone Filmfor High-Precision Solutions, Datasheet of the product available at : https://www.wacker.com/cms/media/publications/downloads/7091_EN.pdf (visited on 19 April 2017).

[19] R. Vertechy, M. Fontana, G. R. Papini, and D. Forehand, "In-tank tests of a dielectric elastomer generator for wave energy harvesting," in SPIE Smart Structures and Materials+Nondestructive Evaluation and Health Monitoring (International Society for Optics and Photonics, 2014) pp. 90561G{90561G.

[20] R. Kaltseis, C. Keplinger, R. Baumgartner, M. Kaltenbrunner, T. Li, P. Machler, R. Schwodiauer, Z. Suo, and S. Bauer, Method for measuring energy generation and efficiency of dielectric elastomer generators," Applied Physics Letters 99, 162904 (2011).

[21] Falnes, J. (2002). Ocean waves and oscillating systems: linear interactions including wave-energy extraction. Cambridge university press.

[22] Evans, D. V. (1981). Maximum wave-power absorption under motion constraints. Applied Ocean Research, 3(4), 200-203.

[23] Pizer, D. J. (1993). Maximum wave-power absorption of point absorbers under motion constraints. Applied Ocean Research, 15(4), 227-234.

[24] M. Righi, R. Vertechy, and M. Fontana, \Experimental characterization of a circular diaphragm dielectric elastomer generator," in ASME 2014 Conference on Smart Materials, Adaptive Structures and Intelligent Systems (American Society of Mechanical Engineers, 2014) pp. V001T03A013{V001T03A013.